THE ASTROPHYSICAL JOURNAL SUPPLEMENT SERIES, 121:369–415, 1999 April

CHEMICAL ABUNDANCES OF THE DAMPED Lyα SYSTEMS AT $z > 1.5$

JASON X. PROCHASKA[1] AND ARTHUR M. WOLFE[1]
Department of Physics and Center for Astrophysics and Space Sciences, University of California, San Diego, C-0424, La Jolla, CA 92093
Received 1998 August 6; accepted 1998 November 12

ABSTRACT

We present chemical abundance measurements for 19 damped Lyα systems observed with the high-resolution echelle spectrograph (HIRES) on the 10 m W.M. Keck Telescope. We perform a detailed analysis of every system, deriving ionic column densities for all unblended metal-line transitions. Our principal goal is to investigate the abundance patterns of the damped systems and thereby determine the underlying physical processes that dominate their chemical evolution. We place particular emphasis on gauging the relative importance of two complementary effects often invoked to explain the damped Lyα abundances (1) nucleosynthetic enrichment from Type II supernovae and (2) an interstellar medium–like (ISM-like) dust-depletion pattern. Similar to the principal results of Lu et al., our observations lend support both for dust depletion and Type II supernova (SN) enrichment. Specifically, the observed overabundance of Zn/Fe and underabundance of Ni/Fe relative to solar abundances suggest significant dust depletion within the damped Lyα systems. Meanwhile, the relative abundances of Al, Si, and Cr versus Fe are consistent with both dust depletion and Type II supernova enrichment. Our measurements of Ti/Fe and the Mn/Fe measurements from Lu et al., however, cannot be explained by dust depletion and indicate an underlying Type II SN pattern. Finally, the observed values of [S/Fe] are inconsistent with the combined effects of dust depletion and the nucleosynthetic yields expected for Type II supernovae. This last result emphasizes the need for another physical process to explain the damped Lyα abundance patterns. We also examine the metallicity of the damped Lyα systems both with respect to Zn/H and Fe/H. Our results confirm previous surveys by Pettini and collaborators, i.e., $[\langle \mathrm{Zn/H} \rangle] = -1.15 \pm 0.15$ dex. In contrast with other damped Lyα surveys at $z > 1.5$, we do not formally observe an evolution of metallicity with redshift, although we stress that this result is based on the statistics from a small sample of high-z damped systems.

Subject headings: galaxies: abundances — intergalactic medium — quasars: absorption lines

1. INTRODUCTION

The damped Lyα systems dominate the neutral gas content of the universe and at high redshift are widely believed to be the progenitors of present-day galaxies (Wolfe et al. 1995). Therefore, one can directly measure the chemical evolution of the early universe by tracing the chemical abundances of the damped systems. Pettini and his collaborators have performed the most extensive surveys on the metallicity of the damped Lyα systems to date (Pettini et al. 1994, 1997). Working on the premise that one can measure accurate column densities of Zn^+ and Cr^+ from unresolved line profiles, they have successfully observed over 30 damped Lyα systems with the Anglo-Australian, William Herschel, and Hale Telescopes. Their results indicate a mean metallicity of Zn/H $\approx$ 1/10 solar abundance with a notably large dispersion. These measurements indicate that the damped systems are chemically young at $z > 2$ and lend further support to the interpretation of damped systems as the progenitors of modern galaxies (e.g., Malaney & Chaboyer 1996). In addition to an analysis of Zn, Pettini et al. performed accurate measurements of $N(Cr^+)$ aided by the coincidence in wavelength of the strongest metal-line transitions for the two species. Comparing the relative abundances of Cr and Zn, they noted an underabundance of Cr to Zn relative to solar abundances (a typical value[2] is [Cr/Zn] ≈ -0.5 dex). In the interstellar medium (ISM), Cr is significantly depleted onto dust grains, whereas Zn is only lightly depleted. Therefore, Pettini and others have argued that the relative underabundance of Cr to Zn is indicative of dust in the damped Lyα systems. They also point out that the Cr/Zn measurements imply a dust-to-gas ratio much lower than that observed in dusty ISM regions where typical values for [Cr/Zn] are less than -1.0 dex. Establishing the level of dust depletion in damped Lyα systems is very important, since dust could significantly bias the results from the damped Lyα surveys against high–N(H I) systems (Fall & Pei 1993).

More recently, Lu et al. (1996) have offered an alternate interpretation for the abundance patterns of the damped systems. Unlike the Pettini et al. sample, Lu et al. measured abundances for a large number of elements including Zn, Cr, Fe, S, N, O, Si, Ni, and Mn with the high-resolution echelle spectrograph (HIRES) on the 10 m W.M. Keck Telescope. The primary result of their analysis is that the damped Lyα systems exhibit abundance patterns typical of nucleosynthetic yields for Type II supernovae. The telltale signature of Type II supernova (SN) enrichment is the overabundance of α-process elements (e.g., Si and S) relative to Fe. Empirical measurements of the abundance patterns for Type II SNe are commonly derived from the metal-poor halo stars (Evardsson et al. 1993) that presumably were primarily enriched by Type II supernovae. As expected for Type II SN abundances, Lu et al. found an overabundance of Si/Fe in every case and further noted that the relative abundances of Fe, Cr, Mn, N, O, and S all match the metal-poor halo star observations. Furthermore, Lu et al. stress that the measured ratios of Mn/Fe and N/O cannot be

[1] Visiting Astronomer, W.M. Keck Telescope. The Keck Observatory is a joint facility of the University of California and the California Institute of Technology.

[2] $[\mathrm{X/Y}] \equiv \log [N(\mathrm{X})/N(\mathrm{Y})] - \log [N(\mathrm{X})/N(\mathrm{Y})]_\odot$

TABLE 1

QSO AND OBSERVATIONAL DATA

QSO	Alternate Name	Date	Exposure Time (s)	z_{em}	Resolution (km s^{-1})	S/N
Q0019−15.....	BR 0019−1522	1996 Feb	35000	4.528	8.0	18
Q0100+13.....	PHL 957	1994 Sep	11700	2.69	8.0	40
Q0149+33.....	OC 383	1997 Feb	17600	2.43	8.0	25
Q0201+36.....	UT 0201+3634	1994 Feb	34580	2.49	8.0	35
Q0347−38.....	...	1996 Feb	12600	3.23	8.0	33
Q0458−02.....	PKS 0458−020	1995 Feb	28800	2.29	8.0	15
Q0841+12.....	...	1997 Feb, 1998 Sep	10800	...	8.0	30
Q0951−04.....	BR 0951−0450	1997 Sep	30600	4.369	8.0	13
Q1215+33.....	GC 1215+3322	1994 Sep	14040	2.61	8.0	20
Q1331+17.....	MC 1331+170	1994 Sep	36000	2.08	6.5	80
Q1346−03.....	BRI 1346−0322	1997 Sep	31000	3.992	8.0	29
Q1759+75.....	GB 1759+7539	1996 Feb	10400	3.05	6.5	33
Q2206−19.....	...	1994 Feb	25900	2.56	8.0	40
Q2230+02.....	LBQS 2230+0232	1997 Feb	18000	2.15	8.0	26
Q2231−00.....	LBQS 2230−0015	1995 Feb	14400	3.02	8.0	30
Q2348−14.....	...	1996 Feb	9000	2.940	8.0	41
Q2359−02.....	UM 196	1997 Feb	25000	2.31	8.0	17

explained in terms of dust depletion and therefore argue for an underlying Type II SN abundance pattern. The interpretation of the damped Lyα abundances patterns as Type II SN enrichment fails, however, with respect to Zn. In particular, the observed overabundance of Zn to Fe (or Cr) contradicts the observations of halo stars where one finds [Zn/Fe] ≈ 0 dex irrespective of the star's metallicity. Although it is possible to theoretically explain the observed overabundance of Zn relative to Fe as a natural consequence of Type II supernova enrichment (Hoffman et al. 1996), the halo star observations pose a significant problem. Several authors have interpreted the observed abundance patterns by combining the effects of dust depletion and Type II SN enrichment (Lu et al. 1996; Kulkarni, Fall, & Truran 1997; Vladilo 1998), but their efforts have been largely unsuccessful. They have had particular difficulty in matching both the [Zn/Fe] and [Mn/Fe] patterns observed in the damped systems. Developing a consistent explanation for all of the abundance patterns remains an outstanding problem.

In this paper we investigate these issues with observations of 19 damped Lyα systems, including two systems previously observed by Lu et al. (1996). Building on the abundance results from Prochaska & Wolfe (1996, 1997a), we derive ionic column densities for all of the unblended metal-line transitions comprising our damped Lyα sample. In turn, we look for abundance patterns similar to those observed in the Lu et al. (1996) sample and interpret these results in the light of dust depletion. Finally, we investigate the evolution of the observed metallicity of the damped Lyα systems with increasing redshift.

In § 2 we summarize the observational sample and data reduction techniques. The individual damped systems are briefly discussed in § 3, and measurements of the ionic column densities and velocity plots of the metal-line transitions are presented. Section 4 discusses the observed abundance patterns of the damped Lyα systems. Finally, the metallicity of the damped Lyα systems is investigated in § 5, and a brief summary is given in § 6.

2. OBSERVATIONAL SAMPLE

Table 1 presents a journal of our observations. In addition to exposure times and dates, we estimate the typical signal-to-noise ratio per pixel (S/N) and resolution of the spectra and include the emission redshift z_{em} of the quasar. All of the data were acquired with HIRES (Vogt 1992) on the 10 m W.M. Keck I telescope. The data were reduced with the HIRES software package developed by T. Barlow. This package converts the two-dimensional echelle images to fully reduced, one-dimensional wavelength-calibrated spectra. We then continuum fitted these spectra with a program similar to the IRAF package *continuum* and optimally co-added multiple observations.

The QSOs in our observational sample all have at least one known intervening damped Lyα system. The systems exhibit a range of N(H I) values and absorption redshifts ($z_{abs} = 1.8$–4.2). In several cases, we have identified additional metal-line systems with very large ionic column densities that suggest that they are damped systems. In the following, however, we restrict our analysis to systems with measured H I column density, $N(\mathrm{H\ I}) > 2 \times 10^{20}$ cm^{-2}. The metal-line transitions are identified by composing velocity plots of the absorption lines listed in Table 2 at the known redshift of the damped system and then correlating the profiles by eye. We performed a systematic search for other metal-line systems toward each QSO to account for possible line misidentification and blending. The data are presented in the following section.

3. IONIC COLUMN DENSITIES

All of the ionic column densities presented in this section were derived with the apparent optical depth method (AODM; Savage & Sembach 1991). Savage & Sembach (1991) have stressed that measuring column densities by fitting multiple Voigt profiles to the line profiles does not always account for hidden saturated components. They introduced a technique to correct for hidden saturation by comparing the apparent column density N_a for multiple transitions from a single ion. The analysis involves calculating $N_a(v)$ for each pixel from the optical depth equation

$$N_a(v) = \frac{m_e c}{\pi e^2} \frac{\tau_a(v)}{f\lambda}, \quad (1)$$

TABLE 2

METAL-LINE DATA

Transition	λ_{rest} (Å)	f[a]
H I λ1215	1215.6701	0.4164
O I λ1302	1302.1685	0.04887
Si II λ1304.....	1304.3702	0.0940
Ni II λ1317.....	1317.217	0.1458[b]
C II λ1334.....	1334.5323	0.1278
Cu II λ1358	1358.773	0.3803
Ni II λ1370.....	1370.131	0.144
Si IV λ1393.....	1393.755	0.528
Sn II λ1400.....	1400.400	0.71
Si IV λ1402.....	1402.770	0.262
Ga II λ1414	1414.402	1.8
Ni II λ1454.....	1454.842	0.0516
Si II λ1526.....	1526.7066	0.1160
C IV λ1548	1548.195	0.1908
C IV λ1550	1550.770	0.09522
Ge II λ1602	1602.4863	0.135
Fe II λ1608.....	1608.4511	0.06196
Fe II λ1611.....	1611.2005	0.001020
Al II λ1670.....	1670.7874	1.88
Pb II λ1682	1682.15	0.156
Ni II λ1703.....	1703.405	0.01224
Ni II λ1709.....	1709.600	0.0666[b]
Ni II λ1741.....	1741.549	0.0776[b]
Ni II λ1751.....	1751.910	0.0638
Si II λ1808.....	1808.0126	0.00218
Al III λ1854	1854.716	0.539
Al III λ1862	1862.790	0.268
Ti II λ1910a	1910.6	0.0975
Ti II λ1910b.....	1910.97	0.0706
Zn II λ2026	2026.136	0.489
Cr II λ2056.....	2056.254	0.1050[c]
Cr II λ2062.....	2062.234	0.0780[c]
Zn II λ2062	2062.664	0.256
Cr II λ2066.....	2066.161	0.05150[c]
Fe II λ2260.....	2260.7805	0.00244
Fe II λ2344.....	2344.214	0.1108
Fe II λ2374.....	2374.4612	0.03260
Fe II λ2382.....	2382.765	0.3006
Mn II λ2576.....	2576.877	0.3508
Fe II λ2586.....	2586.6500	0.0684
Mn II λ2594.....	2594.499	0.2710
Fe II λ2600.....	2600.1729	0.2132
Mn II λ2606.....	2606.462	0.1927

[a] Unless otherwise indicated, the f and λ values were taken from Morton 1991.

[b] Zsargó & Federman 1998.

[c] Tripp et al. 1996.

where $\tau_a(v) = \ln [I_i(v)/I_a(v)]$, f is the oscillator strength, λ is the rest wavelength, and I_i and I_a are the incident and measured intensity. Comparing $N_a(v)$ deduced from two or more transitions of the same ion, one finds the stronger transition will have smaller values of $N_a(v)$ in those features where hidden saturation is present. Thus, one can ascertain the likelihood of saturated components for ions with multiple transitions.

In Wolfe et al. (1994) and Prochaska & Wolfe (1996, 1997a) we showed that the damped Lyα profiles are not contaminated by hidden saturation. Furthermore, we demonstrated that the column densities derived with the AODM agree very well with line-profile fitting, which should give a more accurate measure of the ionic column densities when hidden saturation is negligible. As the AODM is easier to apply to a large data set, we have chosen to use this technique to measure the ionic column densities for the damped Lyα sample. Throughout the paper we adopt the wavelengths and oscillator strengths presented in Table 2 compiled by Morton (1991), Tripp, Lu, & Savage (1996), and Zsargó & Federman (1998).

Tables 3–21 present the results of the abundance measurements, including an estimate of the 1 σ error. For those transitions where the profile saturates (i.e., $I_i/I_a < 0.01$ in at least one pixel), the column densities are listed as lower limits. The values reported as upper limits are 3 σ upper limits. We warn the reader of two points: (1) logarithmic errors are misleadingly small (e.g., a 0.1 dex error is $\approx$25% for a 13 dex measurement) and (2) we have ignored continuum error in our analysis, which could significantly affect measurements of very weak transitions. In the following subsections we comment briefly on each of the damped Lyα systems, plot all of the identified metal-line transitions, and discuss the adopted N(H I) values. We note which systems are members of the Large Bright QSO Survey (LBQS) sample (Wolfe et al. 1995) and advise the reader the refer to that paper for further details. In the velocity plots, $v = 0$ is chosen arbitrarily and corresponds to the redshift listed in the figure legend. We indicate regions where blends with other transitions occur (primarily through blends with other metal-line systems or the Lyα forest) by plotting with dotted lines.

3.1. *Q0000−26*, $z = 3.390$

This high-redshift damped Lyα system has been previously observed with HIRES (Lu et al. 1996), and we adopt log N(H I) = 21.41 ± 0.08 based on that analysis. It is a member of the LBQS (Wolfe et al. 1995) statistical sample,

TABLE 3

IONIC COLUMN DENSITIES: Q0000−26, $z = 3.390$

Ion	λ	AODM	N_{adopt}	[X/H]
H I	1215	21.410 ± 0.080	...	...
C IV	1548	14.707 ± 0.006	...	...
Al III.....	1854	12.772 ± 0.020	...	...
Si II.....	1526	>14.607	15.086 ± 0.012	−1.874 ± 0.081
	1808	15.086 ± 0.012	...	...
Fe II	1611	15.146 ± 0.037	15.146 ± 0.037	−1.774 ± 0.088
Ni II	1751	13.325 ± 0.029	13.325 ± 0.029	−2.335 ± 0.085

TABLE 4

IONIC COLUMN DENSITIES: Q0019−15, $z = 3.439$

Ion	λ	AODM	N_{adopt}	[X/H]
H I	1215	20.900 ± 0.100	...	...
Si II	1526	>14.953	15.423 ± 0.053	-1.027 ± 0.113
	1808	15.423 ± 0.053	...	...
Si IV.....	1402	>14.495	...	...
Fe II.....	1608	14.770 ± 0.064	14.770 ± 0.064	-1.640 ± 0.119
Ni II.....	1709	13.300 ± 0.103	13.442 ± 0.043	-1.708 ± 0.109
	1741	13.442 ± 0.043	...	...

one of the few with $z_{abs} > 3$. The velocity profiles are presented in Figure 1, and the derived ionic column densities are listed in Table 3. As our spectral coverage did not include Fe II λ1608, the Fe abundance is based solely on Fe II λ1611, which is a very weak transition and has a relatively low S/N. Interestingly, we find $N(Fe^+)$ to be significantly higher than the lower limit derived from the Fe II λ1608 transition reported by Lu et al. (1996), which may be the result of an error in the continuum fit to our profile. We find $N(Si^+)$ to be significantly higher as well, however, both from the direct measurement of the Si II λ1808 transition and by fitting a Voigt profile to the saturated Si II λ1526 profile. We therefore note that Lu et al. (1996) may have significantly underestimated the true metallicity. At the same time, we observe that the $N(Ni^+)$ measurement coincides with the Lu et al. results. Because we have no unblended, unsaturated high-S/N profiles for this system we have not included it in the kinematic analyses thus far (Prochaska & Wolfe 1997b; Wolfe & Prochaska 1998; Prochaska & Wolfe 1998).

3.2. *Q0019−15*, $z = 3.439$

This damped Lyα system comes from the high-redshift survey by Storrie-Lombardi et al. (1996), and the adopted $\log N(\text{H I}) = 20.9 \pm 0.1$ was taken from recent Keck measurements of Storrie-Lombardi & Wolfe (1999). Although our observations covered Lyα for this system, the profile extends over two echelle orders and an accurate measurement of N(H I) proved impossible. Figure 2 shows the metal-line transitions and Table 4 presents the measurements for this system. The Fe abundance is based on the marginally saturated Fe II λ1608 profile, yet should be reasonably accurate. The Ni II lines are very weak and in poor S/N regions, so these measurements are not reliable. The same is true for the Si measurements, although to a lesser extent. Note that all of the high-ion profiles are blended with other metal-line transitions or Lyα forest clouds.

3.3. *Q0100+13*, $z = 2.309$

The majority of our results on PHL 957 (Q0100+13) were published by Wolfe et al. (1994). The major exception is that we now present a measurement of the Fe abundance based on the previously unidentified Fe II λ1611 profile. Also, we measure column densities in light of new f and λ values, in particular those for the Cr II and Ni II transitions. Note that the O abundance is based on the very weak O I λ1355 profile and we report it as a 3 σ upper limit. Figure 3 presents the velocity plots and Table 5 lists the measured ionic column densities for this system. This damped system is included in the statistical sample of the LBQS survey.

3.4. *Q0149+33*, $z = 2.140$

This relatively metal-poor ($[Fe/H] \approx -1.8$ dex) damped system is a also member of the LBQS statistical sample. Table 6 gives the measured column densities, and Figure 4 plots the metal lines. In the following analysis, we assume $\log N(\text{H I}) = 20.5 \pm 0.1$ (Wolfe et al. 1995). As with PH 957, the O abundance is based on the statistically insignificant O I λ1355 profile and provides a very conservative upper limit. Finally the Al abundance is derived from the

TABLE 5

IONIC COLUMN DENSITIES: Q0100+13, $z = 2.309$

Ion	λ	AODM	N_{adopt}	[X/H]
H I	1215	21.400 ± 0.050	...	...
C IV	1548	13.241 ± 0.031	...	...
	1550	13.303 ± 0.056	...	...
O I	1355	<17.628	<17.628	<-0.702
Al III.....	1854	12.635 ± 0.022	...	...
	1862	12.715 ± 0.033	...	...
Si II.....	1526	>14.722	>14.722	>-2.228
Si IV	1393	13.127 ± 0.017	...	...
	1402	13.146 ± 0.029	...	...
Cr II	2062	13.389 ± 0.018	13.387 ± 0.015	-1.693 ± 0.052
	2066	13.383 ± 0.024	...	...
Fe II	1608	>14.599	15.096 ± 0.041	-1.814 ± 0.065
	1611	15.096 ± 0.041	...	...
Ni II	1454	13.621 ± 0.041	13.620 ± 0.014	-2.030 ± 0.052
	1741	13.620 ± 0.015	...	...
Zn II.....	2026	12.498 ± 0.028	12.494 ± 0.023	-1.556 ± 0.055
	2062	12.485 ± 0.039	...	...

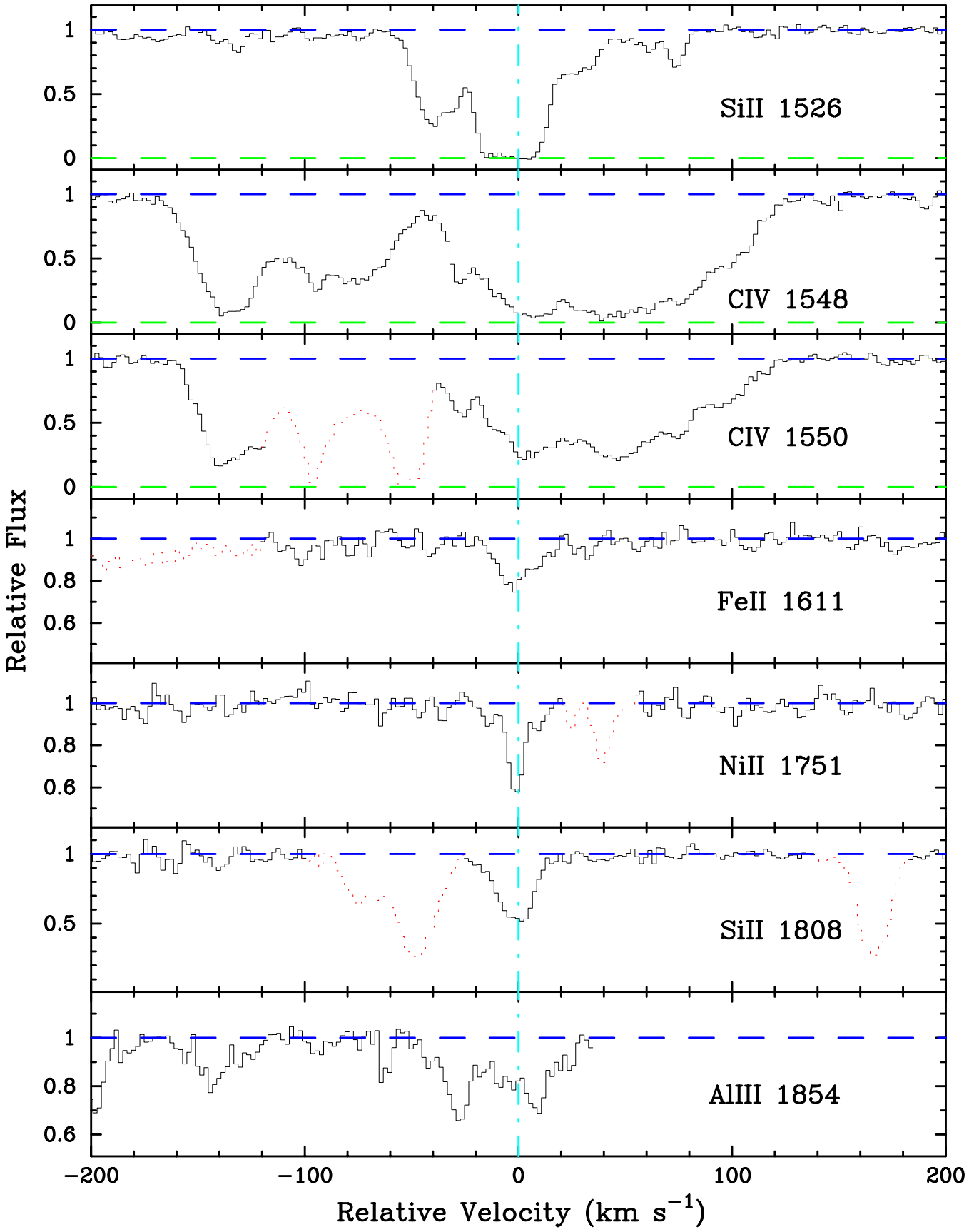

FIG. 1.—Velocity plot of the metal-line transitions for the damped Lyα system at $z = 3.390$ toward Q0000−26. The vertical line at $v = 0$ corresponds to $z = 3.3901$.

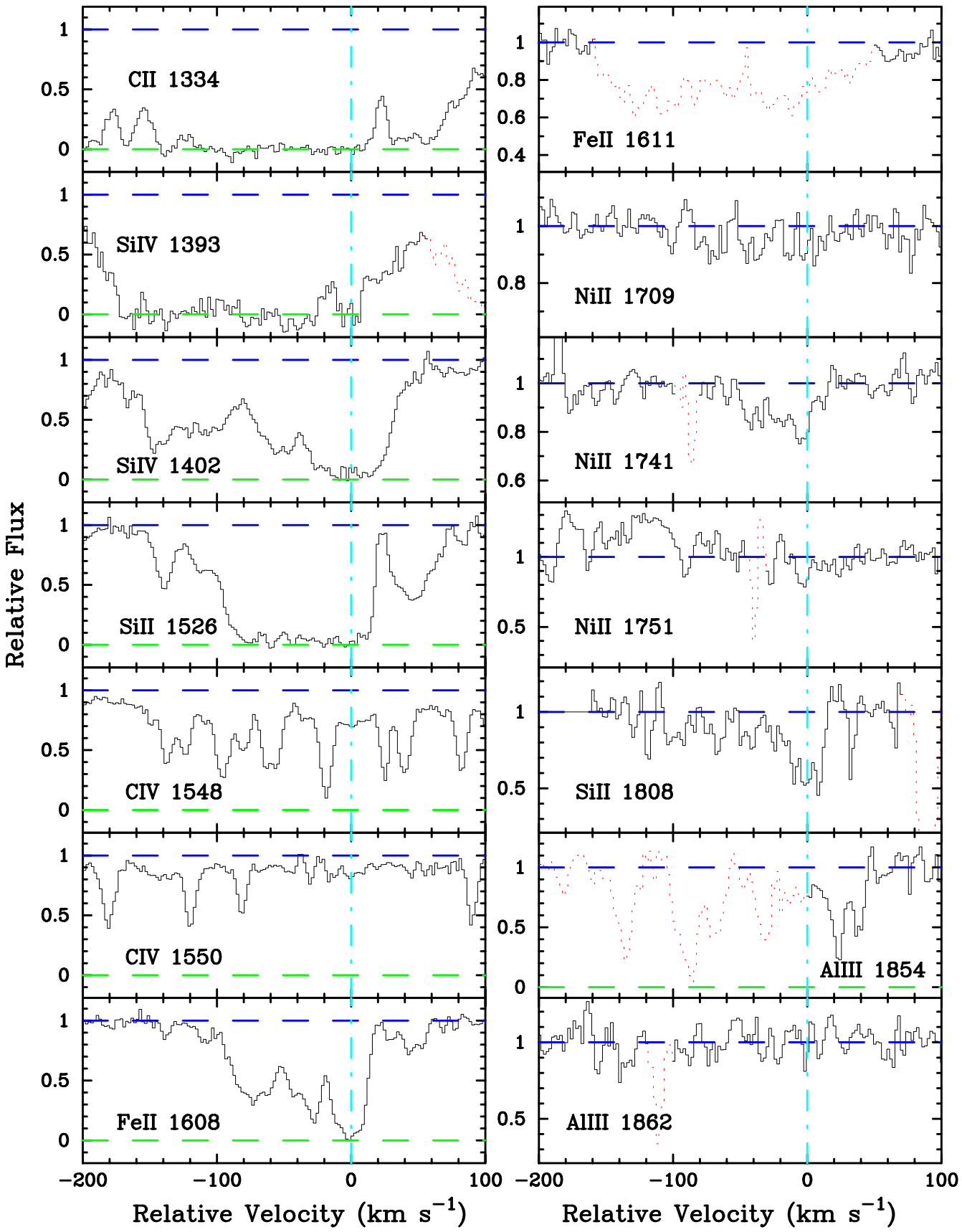

FIG. 2.—Velocity plot of the metal-line transitions for the damped Lyα system at $z = 3.439$ toward Q0019−15. The vertical line at $v = 0$ corresponds to $z = 3.43866$.

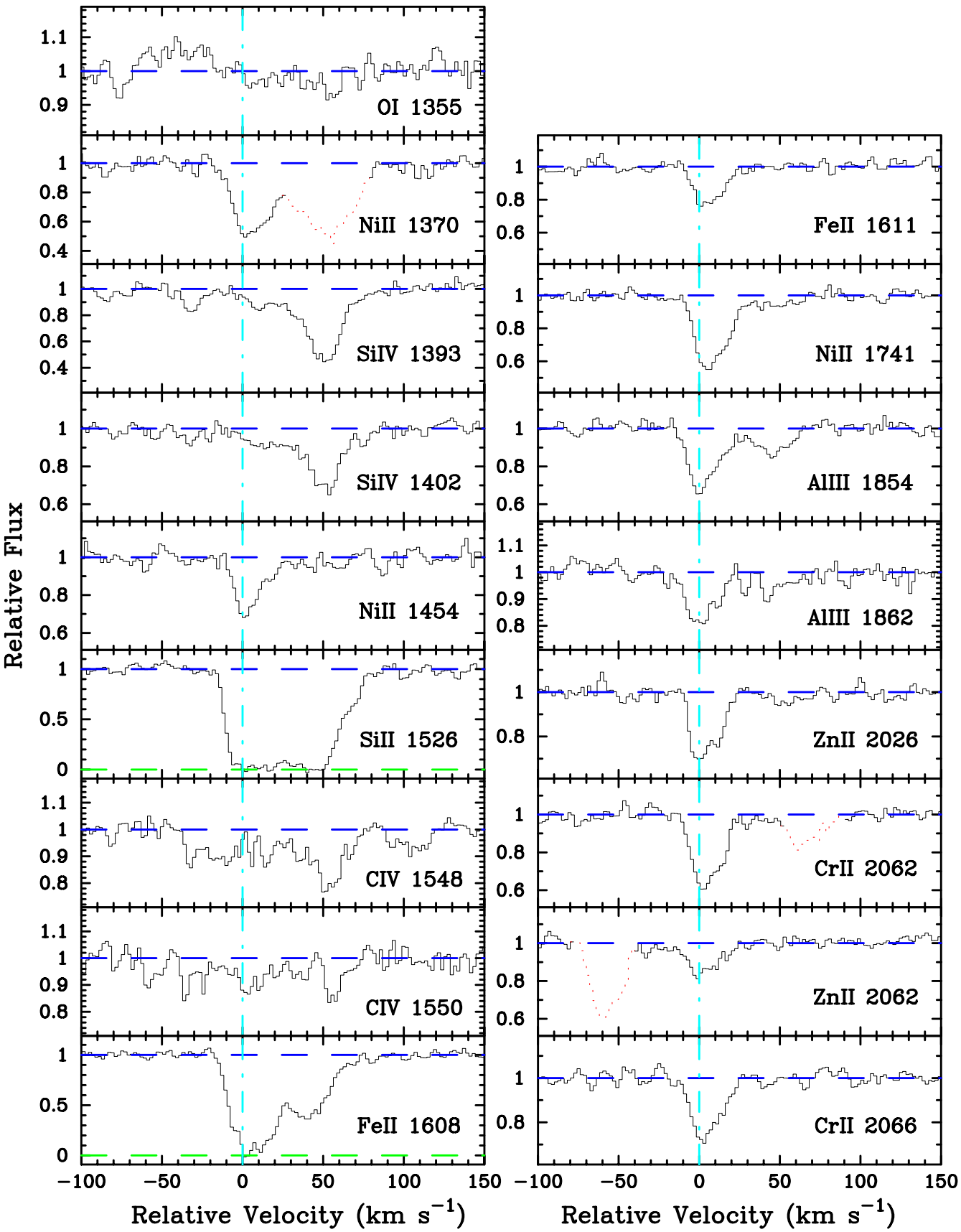

FIG. 3.—Velocity plot of the metal-line transitions for the damped Lyα system at $z = 2.309$ toward Q0100+13. The vertical line at $v = 0$ corresponds to $z = 2.309$.

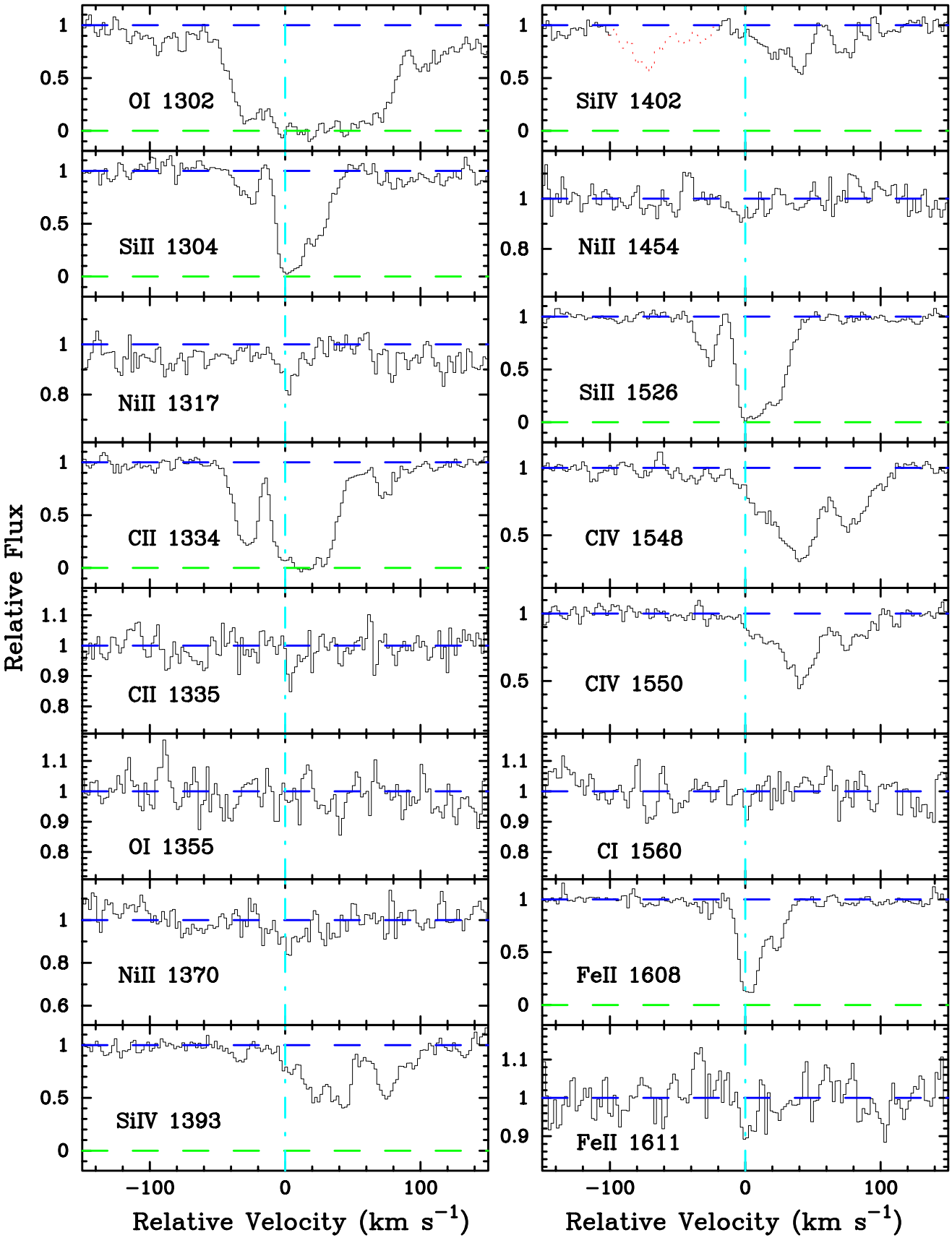

FIG. 4.—Velocity plot of the metal-line transitions for the damped Lyα system at $z = 2.141$ toward Q0149 + 33. The vertical line at $v = 0$ corresponds to $z = 2.140755$.

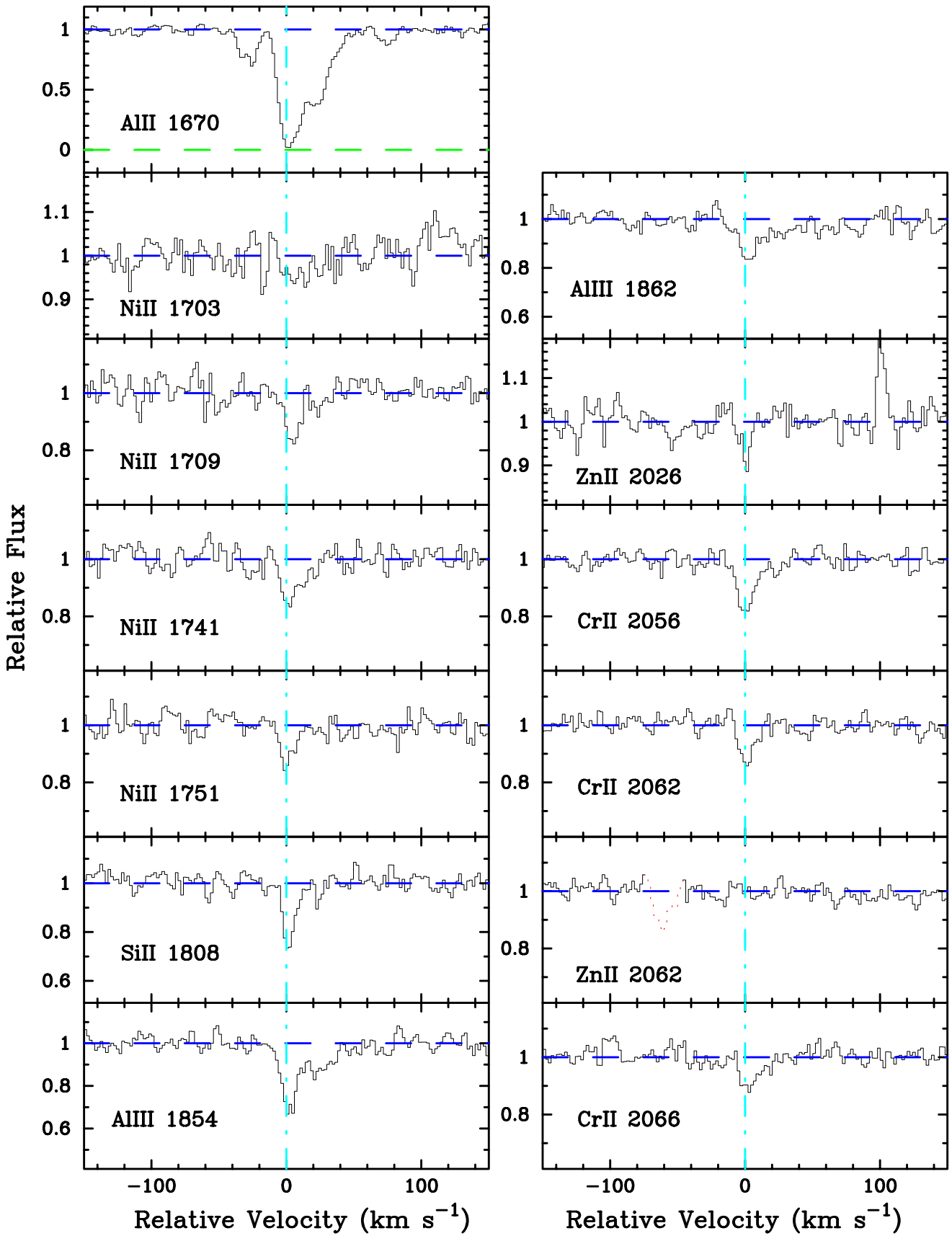

FIG. 4.—*Continued*

TABLE 6

IONIC COLUMN DENSITIES: Q0149+33, $z = 2.140$

Ion	λ	AODM	$N_{\rm adopt}$	[X/H]
H I	1215	20.500 ± 0.100	...	...
C I.....	1560	<12.801	...	...
C II	1334	>14.623	...	...
	1335	<12.780	...	...
C IV	1548	13.880 ± 0.011	...	...
	1550	13.890 ± 0.017	...	...
O I	1355	<17.795	<17.795	<0.365
Al II	1670	12.936 ± 0.018	12.936 ± 0.018	-2.044 ± 0.102
Al III.....	1854	12.518 ± 0.028	...	...
	1862	12.556 ± 0.043	...	...
Si II.....	1304	14.401 ± 0.042	14.367 ± 0.029	-1.683 ± 0.104
	1526	14.320 ± 0.034	...	...
	1808	14.572 ± 0.047	...	...
Si IV	1393	13.380 ± 0.017	...	...
Cr II	2056	12.793 ± 0.044	12.811 ± 0.036	-1.369 ± 0.106
	2062	12.533 ± 0.087	...	...
	2066	12.853 ± 0.060	...	...
Fe II	1608	14.202 ± 0.018	14.202 ± 0.018	-1.808 ± 0.102
	1611	<14.785	...	...
Ni II	1370	12.920 ± 0.103	12.900 ± 0.042	-1.850 ± 0.108
	1703	<13.575	...	...
	1709	12.871 ± 0.088	...	...
	1741	12.990 ± 0.064	...	...
	1751	12.817 ± 0.090	...	...
Zn II.....	2026	11.496 ± 0.103	11.496 ± 0.103	-1.654 ± 0.144
	2062	<11.697	...	...

marginally saturated Al II $\lambda1670$ profile but should be a reliable value. The system is notable for exhibiting an atypical Cr to Zn ratio: [Cr/Zn] $= +0.26 \pm 0.1$ dex. The Cr measurement is reasonably accurate, and the Zn II $\lambda2062$ transition places a rather strict upper limit to the Zn abundance. Therefore, it is very likely [Cr/Zn] > 0 that marks the first such occurrence in a damped system and indicates that this system must be essentially undepleted.

3.5. *Q0347−38*, $z = 3.025$

The damped Lyα system toward Q0347−38 is another member of the LBQS statistical sample, one of the four with $z_{\rm abs} > 3$. We adopt log N(H I) $= 20.8 \pm 0.1$ based on a measurement by Pettini et al. (1994). This is one of the few systems where we have an estimate of $N(S^+)$, although we note that S II $\lambda1259$ is partially blended with the Lyα forest and should be considered an upper limit to the true S abundance, $N(S^+) < 10^{14.73}$ cm^{-2}. We discuss the S/Fe ratio in detail below, noting here that the value has particular impact on interpreting the abundances of the damped Lyα systems with respect to Type II SN enrichment and dust depletion. The system is also notable for the easily identifiable excited fine-structure C II* $\lambda1335$ transition. Unfortunately, the C II $\lambda1334$ profile is so heavily saturated that no meaningful comparison can be made with the fine-structure transition. Finally, we observe a very low Ni abundance for this system, [Ni/H] < -2.37 dex, which implies [Ni/Fe] < -0.5 dex, which may be difficult to explain within the leading explanations for the damped Lyα abundance patterns. Table 7 gives the measured column densities, and Figure 5 plots the metal lines.

3.6. *Q0458−02*, $z = 2.040$

This damped Lyα system is "famous" for exhibiting H I 21 cm absorption. In particular, Briggs et al. (1989) have used VLBI radio observations to place a lower limit on its size of 8 h_{100}^{-1} kpc. In our analysis we adopt log N(H I) $= 21.65 \pm 0.09$ taken from Pettini et al. (1994). A plot of the metal-line profiles is given in Figure 6, and Table 8 lists the column densities. Note that the C II* $\lambda1335$ profile is heavily saturated. Assuming that the $^2P_{3/2}$ excited fine-structure state is populated by e^- collisions and $N(C^+) < 10^{17}$ cm^{-2} (which follows by assuming [C/H] $<$ [Zn/H]), the limit on N(C II*) indicates $n_e > 0.1$ cm^{-3}. The system, with one of the highest measured N(H I) values, must have a high neutral fraction, which implies $n_{\rm H} > 0.1$ cm^{-3}. Because Fe II $\lambda1608$ is saturated, we base the Fe abundance on the Fe II $\lambda1611$ transition. Finally, we note that the Zn II $\lambda2026$ profile is blended with an unidentified line at $v > 20$ km s^{-1} and therefore the AODM was applied only to $v = +20$ km s^{-1}.

3.7. *Q0841+12*, $z = 2.375$ *and* $z = 2.476$

The damped Lyα systems toward this BL Lac object were first identified by C. Hazard and were subsequently analyzed by Pettini et al. (1997). We take N(H I) $= 20.95 \pm 0.087$ for the system at $z = 2.375$ and N(H I) $= 20.78 \pm 0.097$ for the system at $z = 2.476$ (Pettini et al. 1997). Figures 7 and 8 plot the metal-line profiles for these systems and Tables 9 and 10 list the ionic column densities. The profiles for the lower redshift system have good S/N and the derived column densities are accurate. Unfortunately, its Fe II $\lambda1608$ and Fe II $\lambda1611$ transitions are blended with sky lines. In the abundance analysis, then, we will adopt an Fe abundance, [Fe/H] = [Cr/H], motivated by the fact that [Cr/Fe] ≈ 0 in the damped systems. For the system at $z = 2.476$, Si II $\lambda1808$ is blended with the Al III $\lambda1862$ transition from the $z = 2.375$ system and may be contaminated by a sky line. Therefore, we adopt a lower

TABLE 7

IONIC COLUMN DENSITIES: Q0347−38, $z = 3.025$

Ion	λ	AODM	N_{adopt}	[X/H]
H I	1215	20.800 ± 0.100	...	...
C II.....	1334	>15.027	>15.027	>-2.333
	1335	13.477 ± 0.032	...	...
C IV	1548	13.846 ± 0.011	...	...
	1550	13.783 ± 0.020	...	...
O I	1302	>15.379	<17.740	<0.010
	1355	<17.740	...	...
Si II	1260	>14.268	14.820 ± 0.028	-1.530 ± 0.104
	1304	14.820 ± 0.028	...	...
	1526	>14.748	...	...
Si IV.....	1393	13.750 ± 0.017	...	...
S II	1259	14.731 ± 0.012	14.731 ± 0.012	-1.339 ± 0.101
Fe II.....	1608	14.472 ± 0.007	14.472 ± 0.007	-1.838 ± 0.100
	1611	<14.476	...	...
Ni II.....	1370	<12.677	<12.677	<-2.373

limit to $N(Si^+)$ from the saturated Si II λ1526 profile. Finally, we obtain an upper limit measurement for $N(Zn^+)$ for this system, which is a significant improvement over previous efforts (Pettini et al. 1997).

3.8. *Q0951−04, $z = 3.857$ and $z = 4.203$*

The QSO Q0951−04 from the survey by Storrie-Lombardi et al. (1996) has two intervening damped Lyα systems, both at very high redshift. The velocity plots and measurements for the $z = 3.857$ system are given in Figure 9 and Table 11, whereas those for the $z = 4.203$ system are presented by Figure 10 and Table 12. We adopt log N(H I) = 20.6 ± 0.1 for the system at $z = 3.857$ and log N(H I) = 20.4 ± 0.1 for the system at $z = 4.203$, based on recent Keck measurements (Storrie-Lombardi & Wolfe 1999). Because all of the column densities are based on either marginally saturated profiles or weaker, low S/N profiles, all of these measurements are somewhat tentative. In fact, we consider the limits on $N(Fe^+)$ for the system at $z = 4.203$ to be too conservative to include this system in the abundance analysis. Finally, we note that the feature at $v = 180$ km s^{-1} in the Ni II λ1370 profile for the $z = 3.857$ system may be an unidentified blend, although it nearly coincides with a strong feature in the Si II λ1526 profile.

3.9. *Q1215+33, $z = 1.999$*

This radio-selected damped system (Wolfe et al. 1986) was observed as part of the commissioning run for the HIRES instrument and is a member of the LBQS statistical sample. In the following analysis we assume log N(H I) = 20.95 ± 0.067 based on observations by Pettini et al. (1994). Figure 11 presents a plot of the metal-line tran-

TABLE 8

IONIC COLUMN DENSITIES: Q0458−02, $z = 3.040$

Ion	λ	AODM	N_{adopt}	[X/H]
H I	1215	21.650 ± 0.090	...	...
C II	1334	>15.010	...	...
	1335	>14.794	...	...
C IV	1548	>14.906	...	...
	1550	>15.111	...	...
O I	1302	>15.410	...	...
	1355	<18.560	...	...
Al II	1670	>13.720	...	...
Al III.....	1854	13.334 ± 0.018	...	...
	1862	13.335 ± 0.022	...	...
Si II.....	1304	>15.095	>15.095	>-2.105
	1526	>14.981	...	...
	1808	>16.021	...	...
Si IV	1393	>14.262	...	...
	1402	>14.481	...	...
Cr II	2056	13.756 ± 0.013	13.797 ± 0.008	-1.533 ± 0.090
	2062	13.763 ± 0.014	...	...
	2066	13.987 ± 0.015	...	...
Fe II	1608	>15.136	15.508 ± 0.048	-1.652 ± 0.102
	1611	15.508 ± 0.048	...	...
Ni II	1317	13.985 ± 0.024	13.853 ± 0.019	-2.047 ± 0.092
	1709	13.840 ± 0.035	...	...
	1741	13.936 ± 0.032	...	...
	1751	13.808 ± 0.033	...	...
Zn II.....	2026	13.141 ± 0.018	13.141 ± 0.018	-1.159 ± 0.092

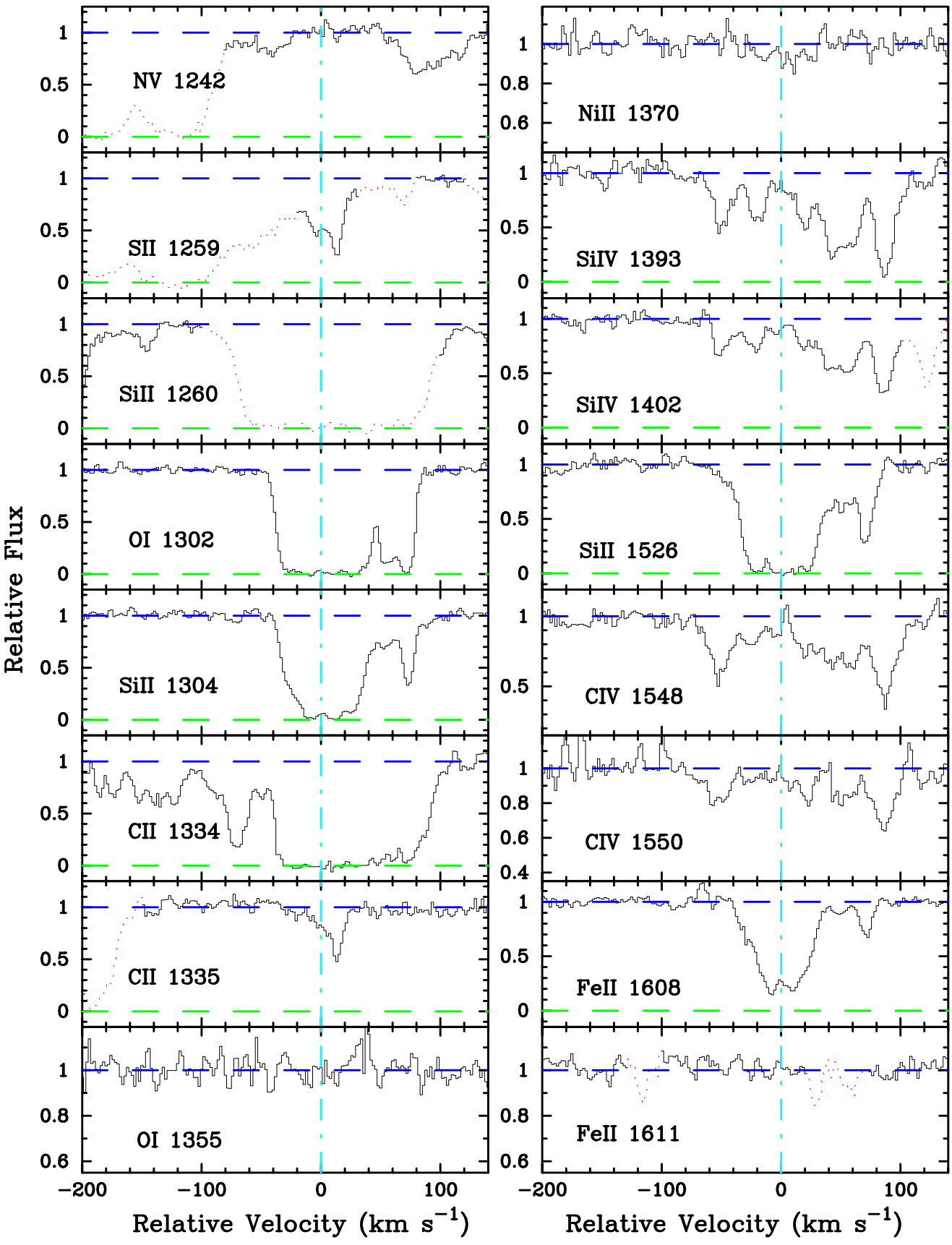

FIG. 5.—Velocity plot of the metal-line transitions for the damped Lyα system at $z = 3.025$ toward Q0347−38. The vertical line at $v = 0$ corresponds to $z = 3.0247$.

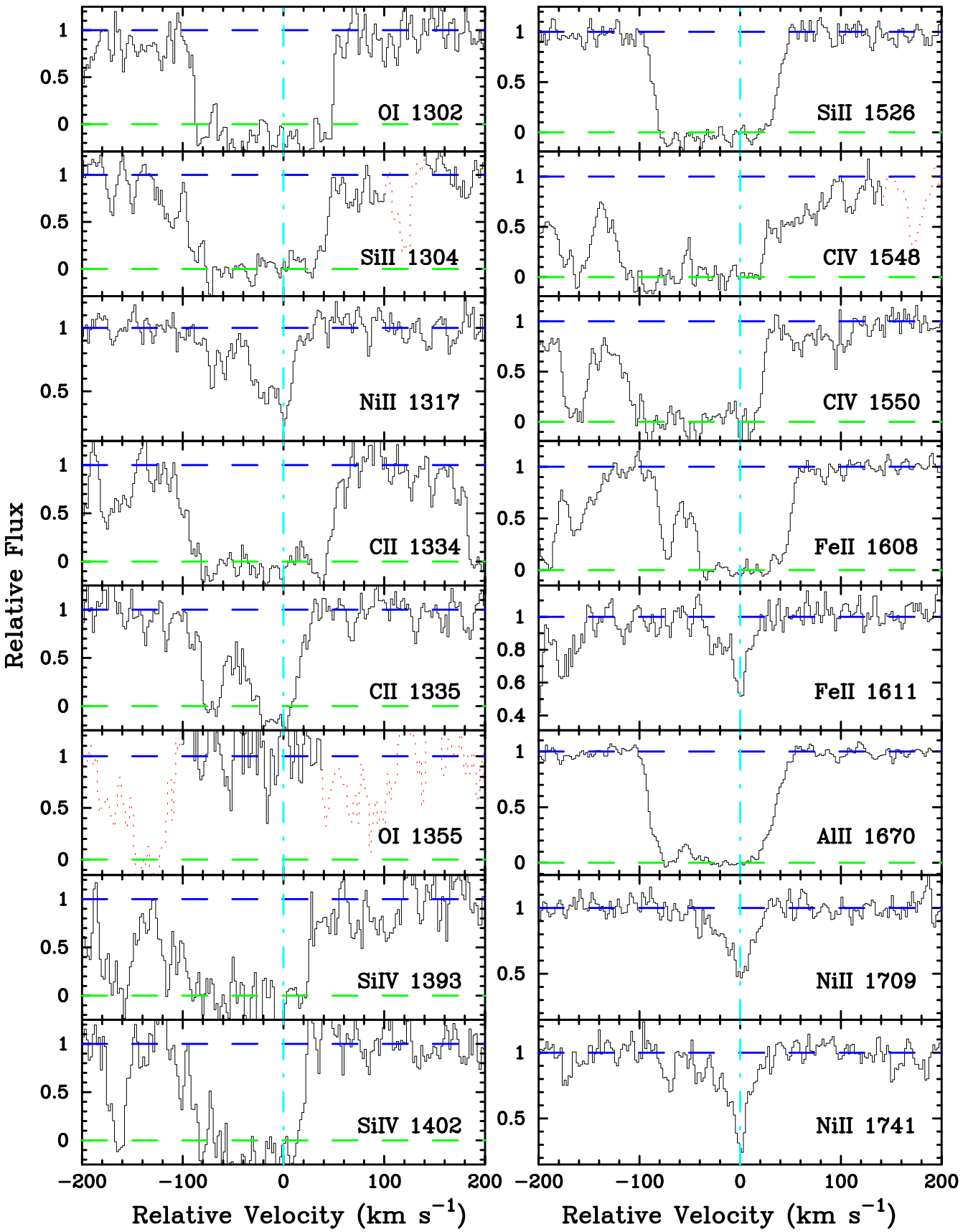

FIG. 6.—Velocity plot of the metal-line transitions for the damped Lyα system at $z = 2.040$ toward Q0458 − 02. The vertical line at $v = 0$ corresponds to $z = 2.03955$.

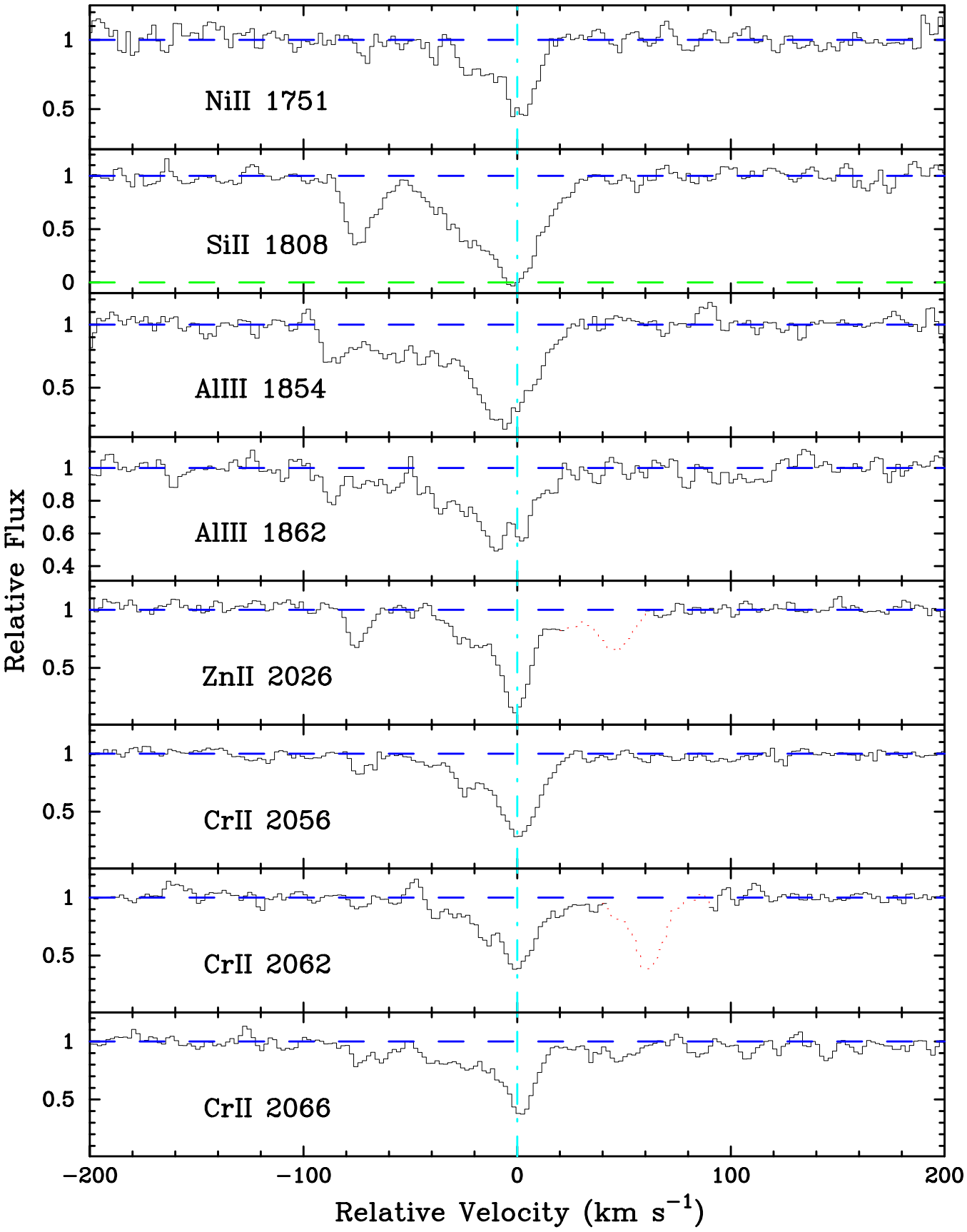

FIG. 6.—*Continued*

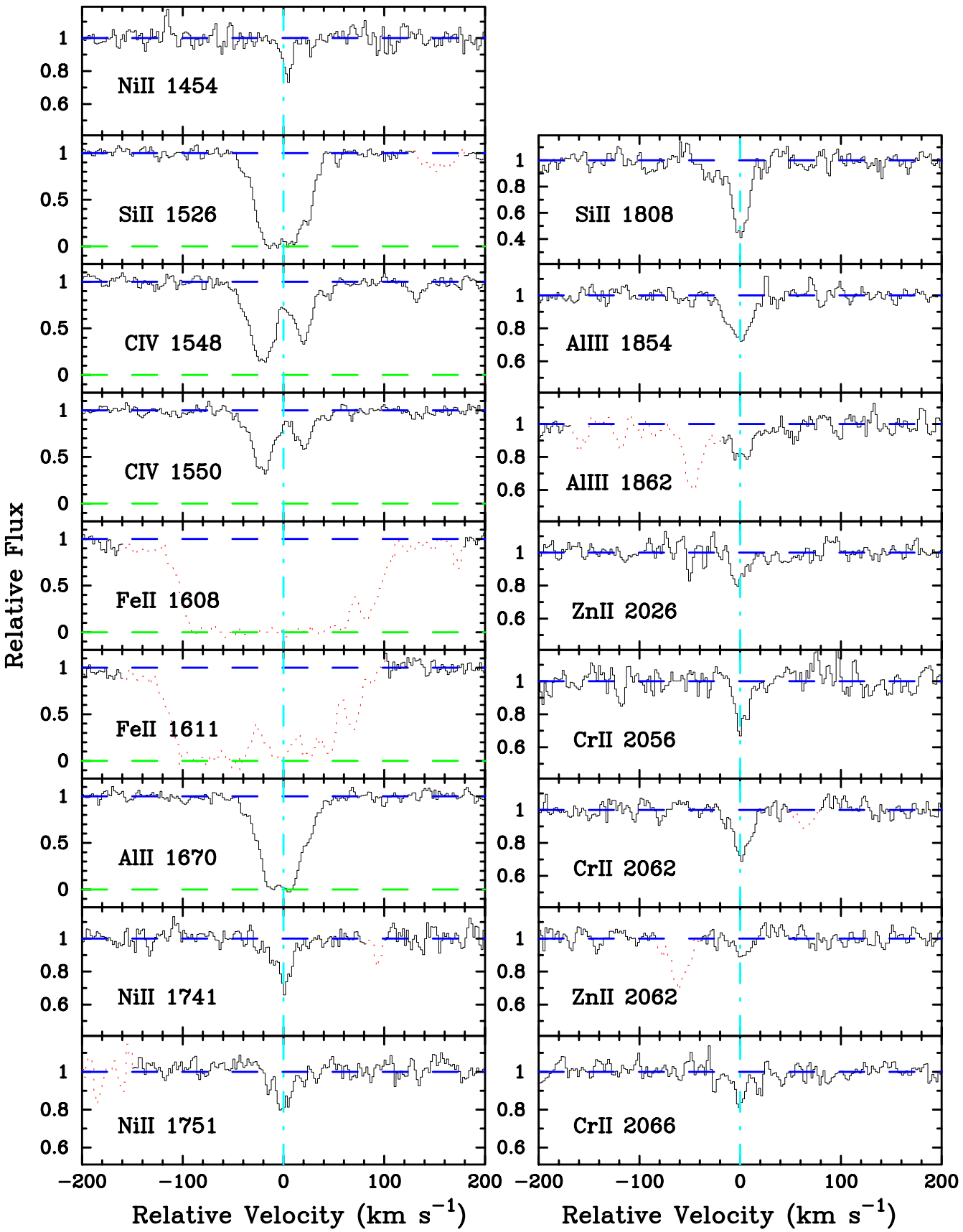

FIG. 7.—Velocity plot of the metal-line transitions for the damped Lyα system at $z = 2.374$ toward Q0841+12. The vertical line at $v = 0$ corresponds to $z = 2.374518$.

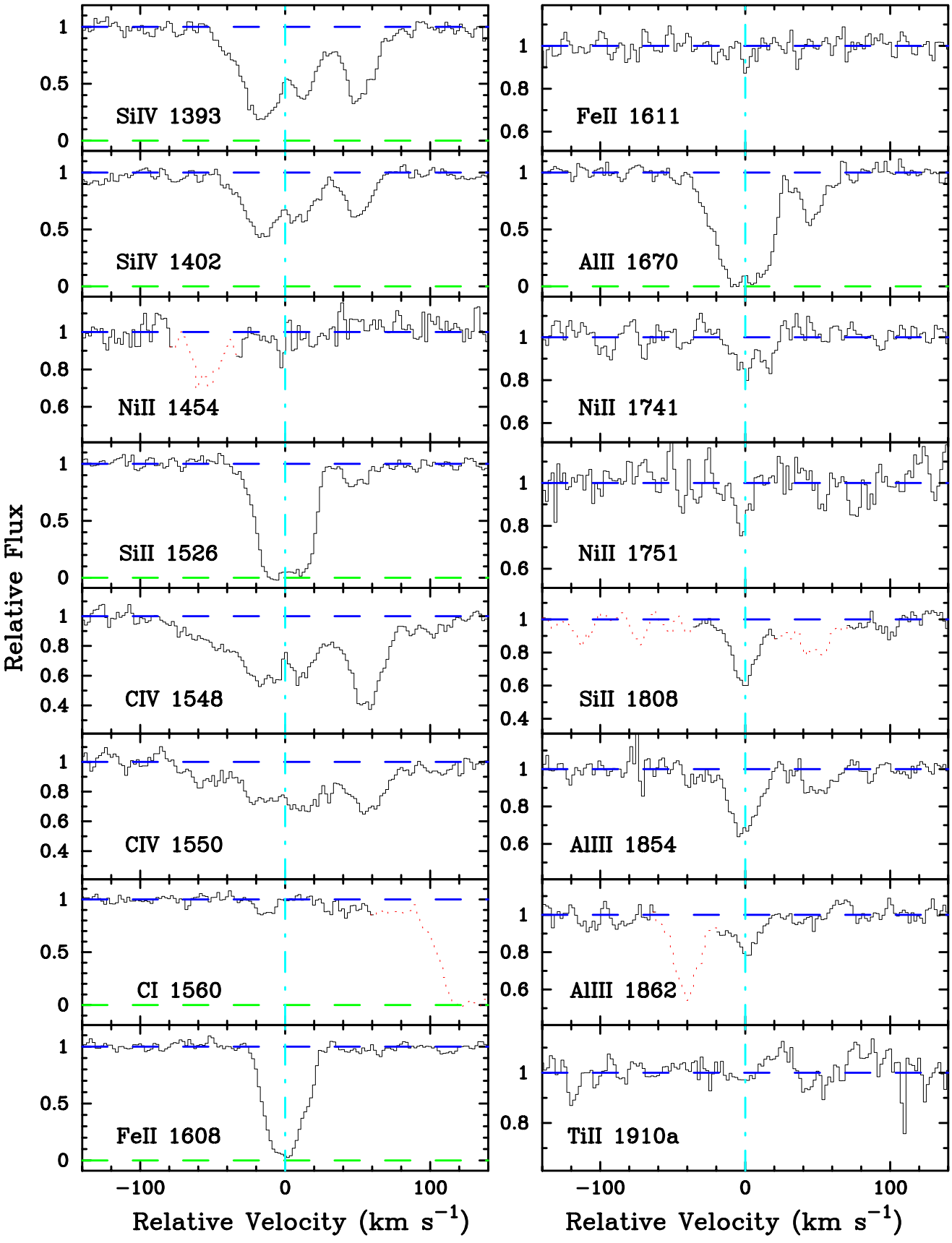

FIG. 8.—Velocity plot of the metal-line transitions for the damped Lyα system at $z = 2.476$ toward Q0841 + 12. The vertical line at $v = 0$ corresponds to $z = 2.476219$.

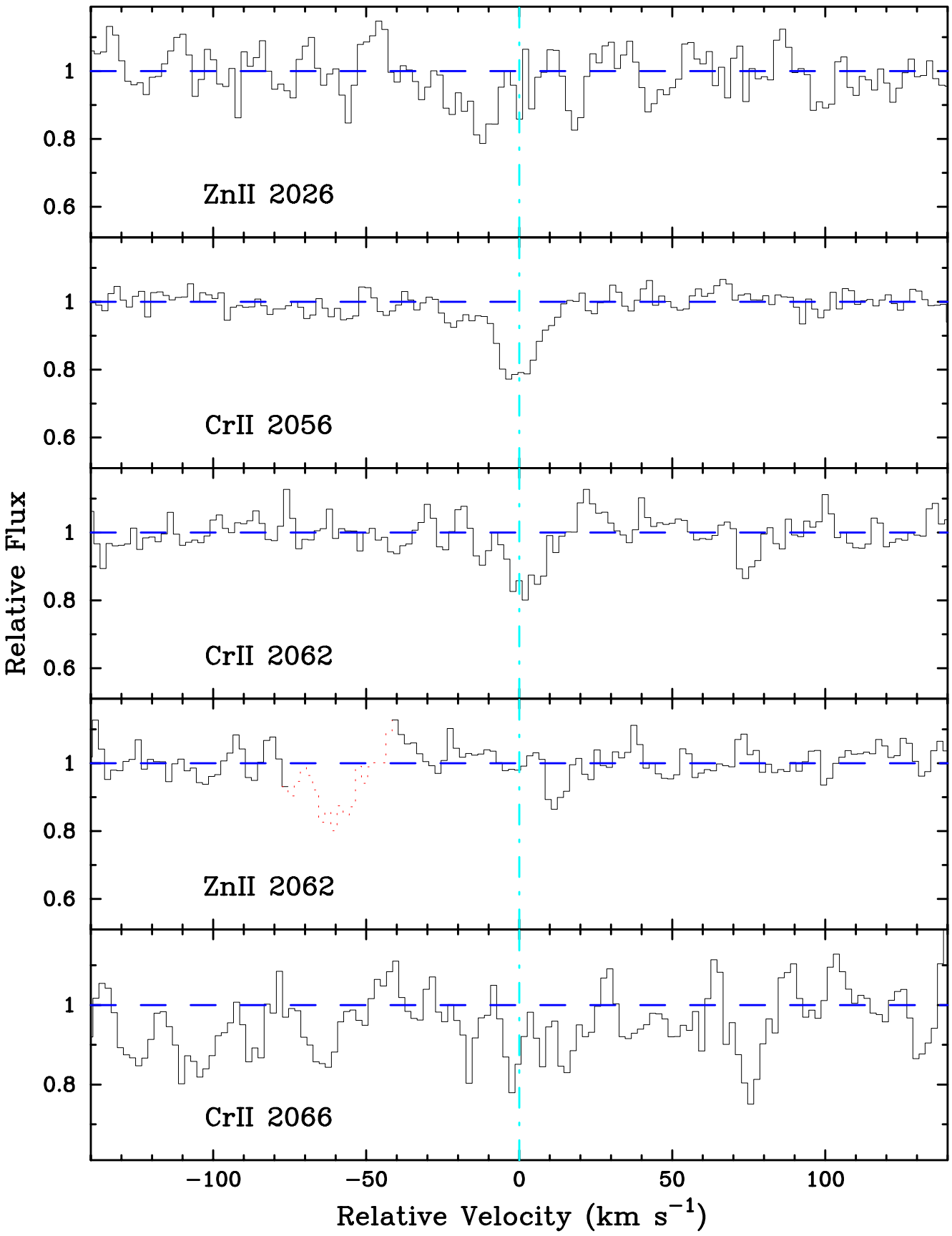

FIG. 8.—*Continued*

TABLE 9

IONIC COLUMN DENSITIES: Q0841+12, $z = 2.375$

Ion	λ	AODM	N_{adopt}	[X/H]
H I	1215	20.950 ± 0.087	...	...
C IV	1548	13.968 ± 0.011	...	...
	1550	13.973 ± 0.015	...	...
Al II	1670	>13.267	>13.267	>-2.163
Al III.....	1854	12.504 ± 0.029	...	...
	1862	12.703 ± 0.035	...	...
Si II.....	1526	>14.566	15.239 ± 0.024	-1.261 ± 0.090
	1808	15.239 ± 0.024	...	...
Cr II	2056	12.960 ± 0.061	13.079 ± 0.027	-1.551 ± 0.091
	2062	13.185 ± 0.034	...	...
	2066	13.035 ± 0.059	...	...
Ni II	1454	13.211 ± 0.075	13.243 ± 0.030	-1.957 ± 0.092
	1741	13.297 ± 0.039	...	...
	1751	13.185 ± 0.055	...	...
Zn II.....	2026	12.114 ± 0.057	12.115 ± 0.049	-1.485 ± 0.100
	2062	12.115 ± 0.099	...	...

sitions, and the ionic column densities are listed in Table 13. Since the Fe II λ1608 profile is saturated and the Fe II λ1611 transition is marginally detected, we establish only a lower limit to $N(Fe^+)$. We will include this system in the abundance analysis, however, by adopting $\log 10[N(Fe^+)] = 14.648 \pm 0.033$ based solely on the Fe II λ1608 profile, noting that this value may be an underestimate.

3.10. *Q1331+17*, $z = 1.776$

This famous damped Lyα system that exhibits 21 cm absorption (Wolfe & Davis 1979) has been studied by a number of authors (over 100 papers), yet never with the quality of data presented here (FWHM resolution ≈ 6 km s^{-1} and S/N > 50). Table 14 lists the column densities for the metal-line transitions, and Figure 12 plots their profiles.

TABLE 10

IONIC COLUMN DENSITIES: Q0841+12, $z = 2.476$

Ion	λ	AODM	N_{adopt}	[X/H]
H I	1215	20.780 ± 0.097	...	...
C IV	1548	13.914 ± 0.009	...	...
	1550	13.986 ± 0.012	...	...
Al II	1670	13.186 ± 0.286	13.186 ± 0.286	-2.074 ± 0.302
Al III.....	1854	12.683 ± 0.027	...	...
	1862	12.633 ± 0.038	...	...
Si II.....	1526	>14.461	>14.461	>-1.869
	1808	14.958 ± 0.022	...	...
Si IV	1393	13.646 ± 0.009	...	...
	1402	13.646 ± 0.011	...	...
Ti II	1910	<12.434	<12.434	<-1.276
Cr II	2056	12.907 ± 0.043	12.840 ± 0.036	-1.620 ± 0.103
	2062	12.759 ± 0.061	...	...
	2066	<12.802	...	...
Fe II	1608	14.434 ± 0.027	14.434 ± 0.027	-1.856 ± 0.101
	1611	<14.668	...	...
Ni II	1741	13.067 ± 0.052	13.048 ± 0.049	-1.982 ± 0.108
	1751	12.965 ± 0.129	...	...
Zn II.....	2026	<11.778	<11.778	<-1.652
	2062	<11.772	...	...

TABLE 11

IONIC COLUMN DENSITIES: Q0951−04, $z = 3.857$

Ion	λ	AODM	N_{adopt}	[X/H]
H I	1215	20.600 ± 0.100	...	...
Al II	1670	13.298 ± 0.022	13.298 ± 0.022	-1.782 ± 0.102
Si II	1526	14.645 ± 0.030	14.645 ± 0.030	-1.505 ± 0.104
Si IV.....	1393	13.900 ± 0.011	...	...
Fe II.....	1608	14.062 ± 0.060	14.062 ± 0.060	-2.048 ± 0.117
Ni II.....	1370	12.994 ± 0.099	12.994 ± 0.099	-1.856 ± 0.141

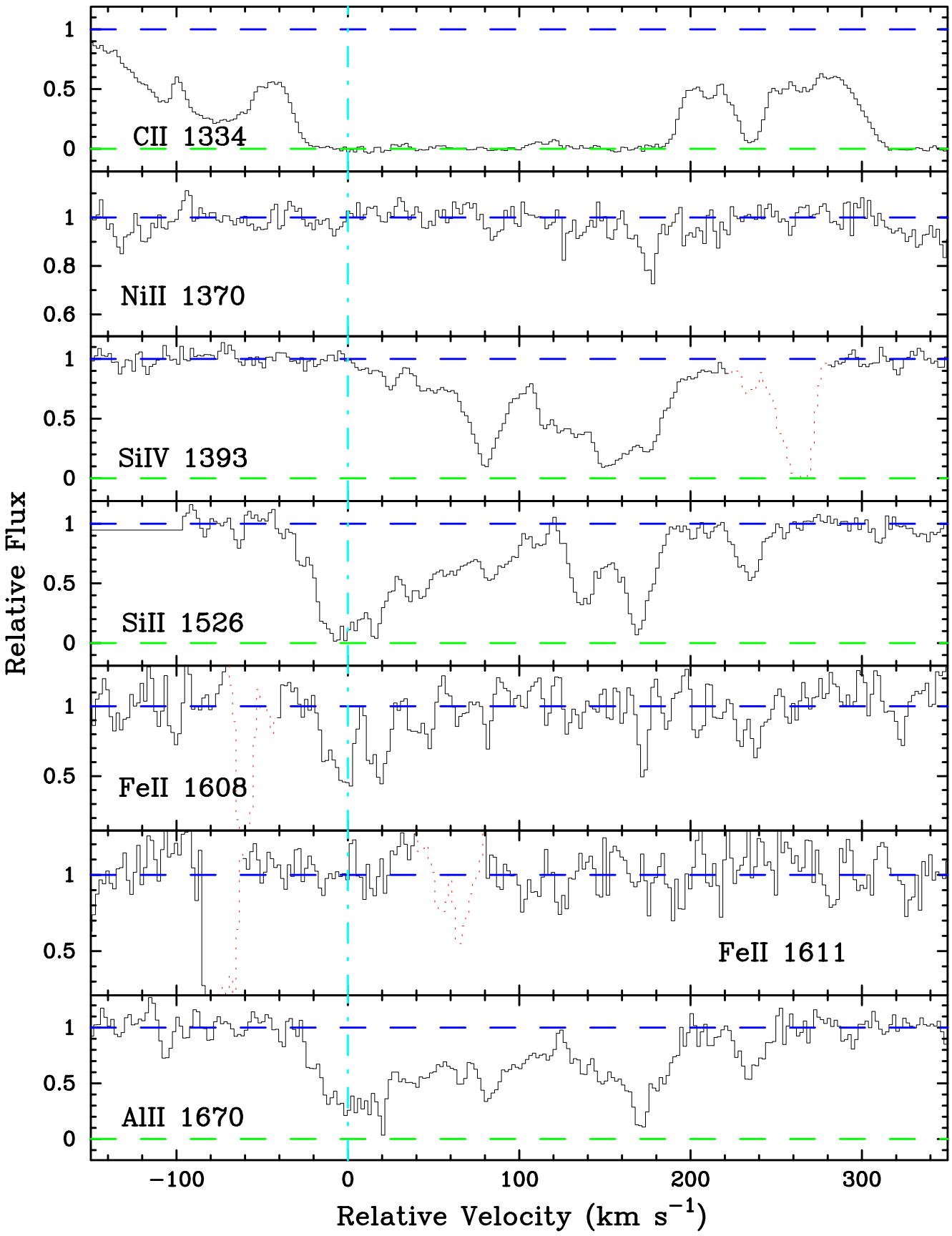

FIG. 9.—Velocity plot of the metal-line transitions for the damped Lyα system at $z = 3.386$ toward Q0951−04. The vertical line at $v = 0$ corresponds to $z = 3.856689$.

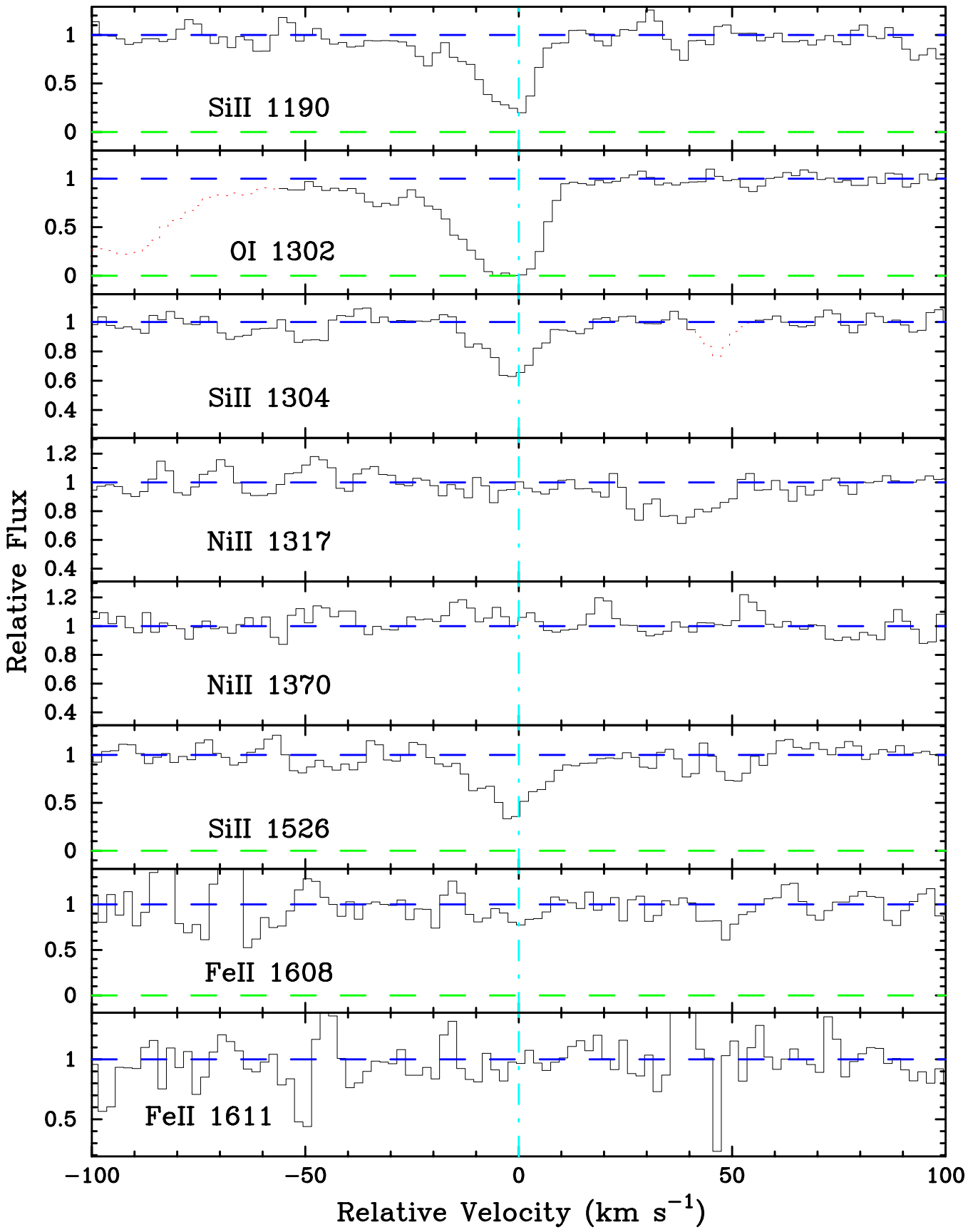

FIG. 10.—Velocity plot of the metal-line transitions for the damped Lyα system at $z = 4.203$ toward Q0951−04. The vertical line at $v = 0$ corresponds to $z = 4.202896$.

TABLE 12

IONIC COLUMN DENSITIES: Q0951−04, $z = 4.203$

Ion	λ	AODM	N_{adopt}	[X/H]
H I	1215	20.400 ± 0.100	...	...
O I	1302	14.607 ± 0.323	14.607 ± 0.323	-2.723 ± 0.339
Si II	1190	13.455 ± 0.050	13.392 ± 0.032	-2.558 ± 0.105
	1304	13.286 ± 0.060	...	...
	1526	13.483 ± 0.055	...	...
Fe II.....	1608	<13.281	<13.281	<-2.629
	1611	<15.153	...	...
Ni II.....	1317	<12.589	<12.589	<-2.061
	1370	<12.625	...	...

We assume log N(H I) = 21.176 ± 0.041 (Pettini et al. 1994). The S/N is excellent throughout the entire spectrum, which yields very accurate column density measurements. This is one of the very few systems where C I absorption is detected, and Songaila et al. (1994) have used measurements of the C I profile to estimate the cosmic background temperature at $z = 1.776$. Consider the feature at $v = +20$ km s^{-1}, which is fully resolved in the C I profiles, barely resolved in the Zn^+

TABLE 13

IONIC COLUMN DENSITIES: Q1215+33, $z = 1.999$

Ion	λ	AODM	N_{adopt}	[X/H]
H I	1215	20.950 ± 0.067	...	...
C IV	1548	13.605 ± 0.019	...	...
	1550	13.672 ± 0.030	...	...
O I	1355	<17.952	<17.952	<0.072
Al II	1670	>13.358	...	...
Al III.....	1854	12.746 ± 0.017	...	...
	1862	12.783 ± 0.021	...	...
Si II.....	1526	>14.681	15.030 ± 0.025	-1.470 ± 0.072
	1808	15.030 ± 0.025	...	...
Si IV	1393	12.993 ± 0.039	...	...
Cr II	2056	13.173 ± 0.034	13.130 ± 0.031	-1.500 ± 0.074
	2062	13.034 ± 0.066	...	...
Fe II	1608	14.648 ± 0.039	14.648 ± 0.039	-1.812 ± 0.078
	1611	14.925 ± 0.100	...	...
Ni II	1741	13.419 ± 0.040	13.344 ± 0.033	-1.856 ± 0.075
	1751	13.262 ± 0.056	...	...
Zn II.....	2026	12.291 ± 0.058	12.291 ± 0.058	-1.309 ± 0.089

TABLE 14

IONIC COLUMN DENSITIES: Q1331+17, $z = 1.776$

Ion	λ	AODM	N_{adopt}	[X/H]
H I	1215	21.176 ± 0.041	...	...
C I.....	1560	13.573 ± 0.013	...	...
	1656	13.312 ± 0.012	...	...
C IV	1548	>15.073	...	...
	1550	>15.172	...	...
Al II	1670	>13.573	...	...
Al III.....	1854	13.004 ± 0.004	...	...
	1862	12.968 ± 0.007	...	...
Si II.....	1526	>14.951	15.285 ± 0.004	-1.441 ± 0.041
	1808	15.285 ± 0.004	...	...
Cr II	2056	12.950 ± 0.017	12.919 ± 0.015	-1.937 ± 0.044
	2066	12.834 ± 0.034	...	...
Fe II	1608	14.601 ± 0.003	14.598 ± 0.001	-2.088 ± 0.041
	2344	14.597 ± 0.022	...	...
	2374	14.598 ± 0.002	...	...
	2382	>14.433	...	...
Ni II	1709	13.166 ± 0.017	13.235 ± 0.009	-2.191 ± 0.042
	1741	13.313 ± 0.011	...	...
	1751	13.165 ± 0.022	...	...
Zn II.....	2026	12.605 ± 0.009	12.605 ± 0.008	-1.221 ± 0.042
	2062	12.605 ± 0.013	...	...

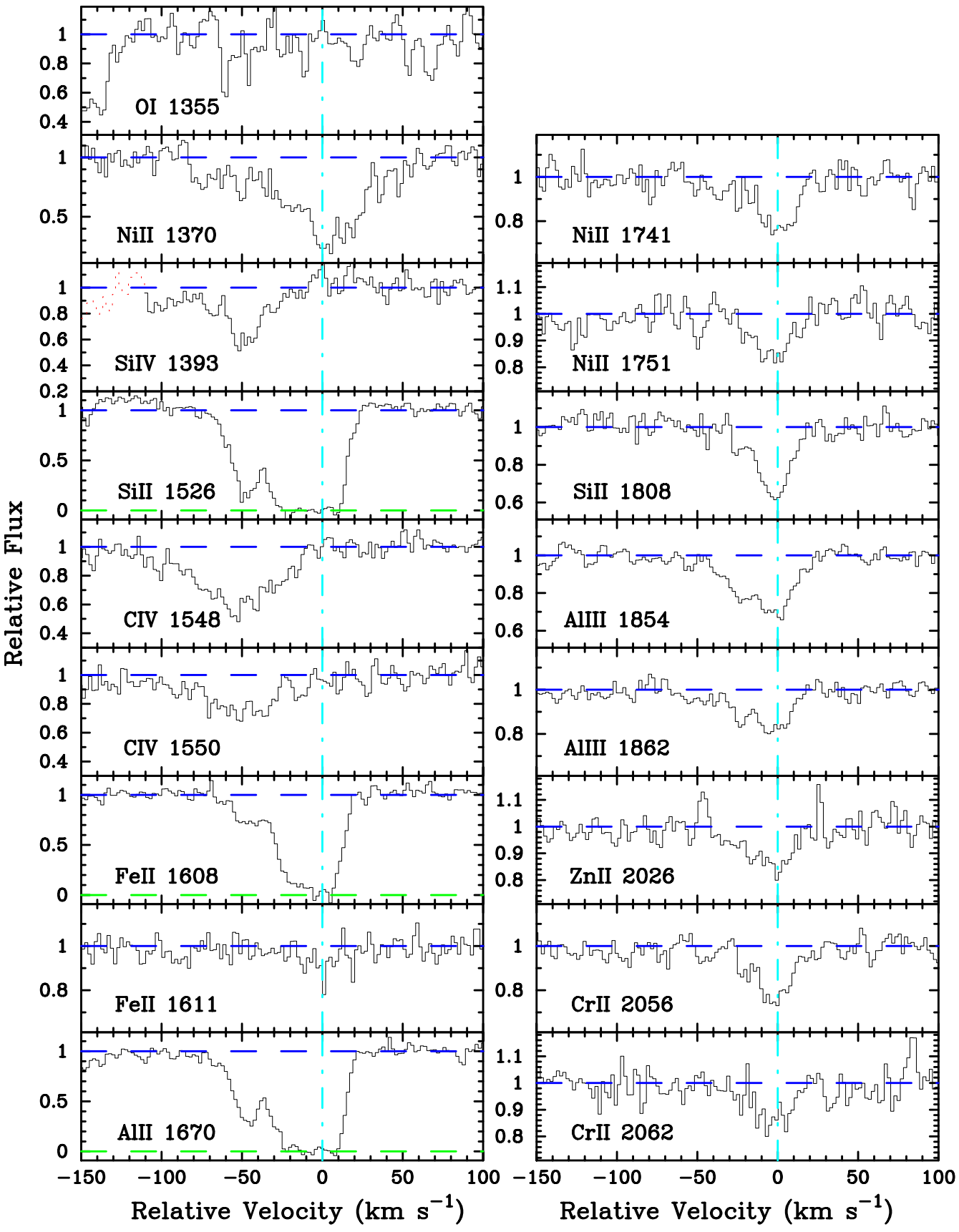

FIG. 11.—Velocity plot of the metal-line transitions for the damped Lyα system at $z = 1.999$ toward Q1215+33. The vertical line at $v = 0$ corresponds to $z = 1.9991$.

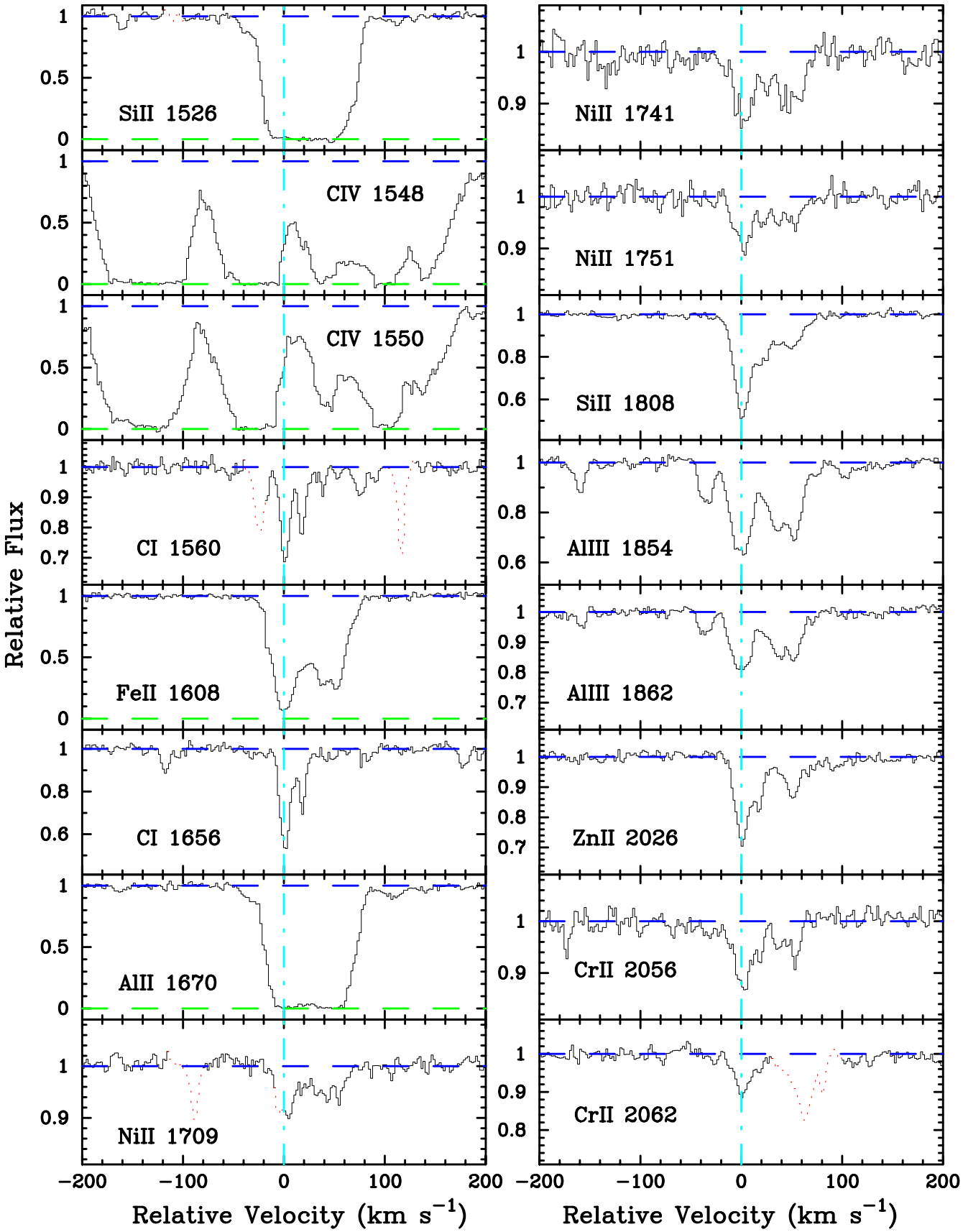

FIG. 12.—Velocity plot of the metal-line transitions for the damped Lyα system at $z = 1.776$ toward Q1331 + 17. The vertical line at $v = 0$ corresponds to $z = 1.77636$.

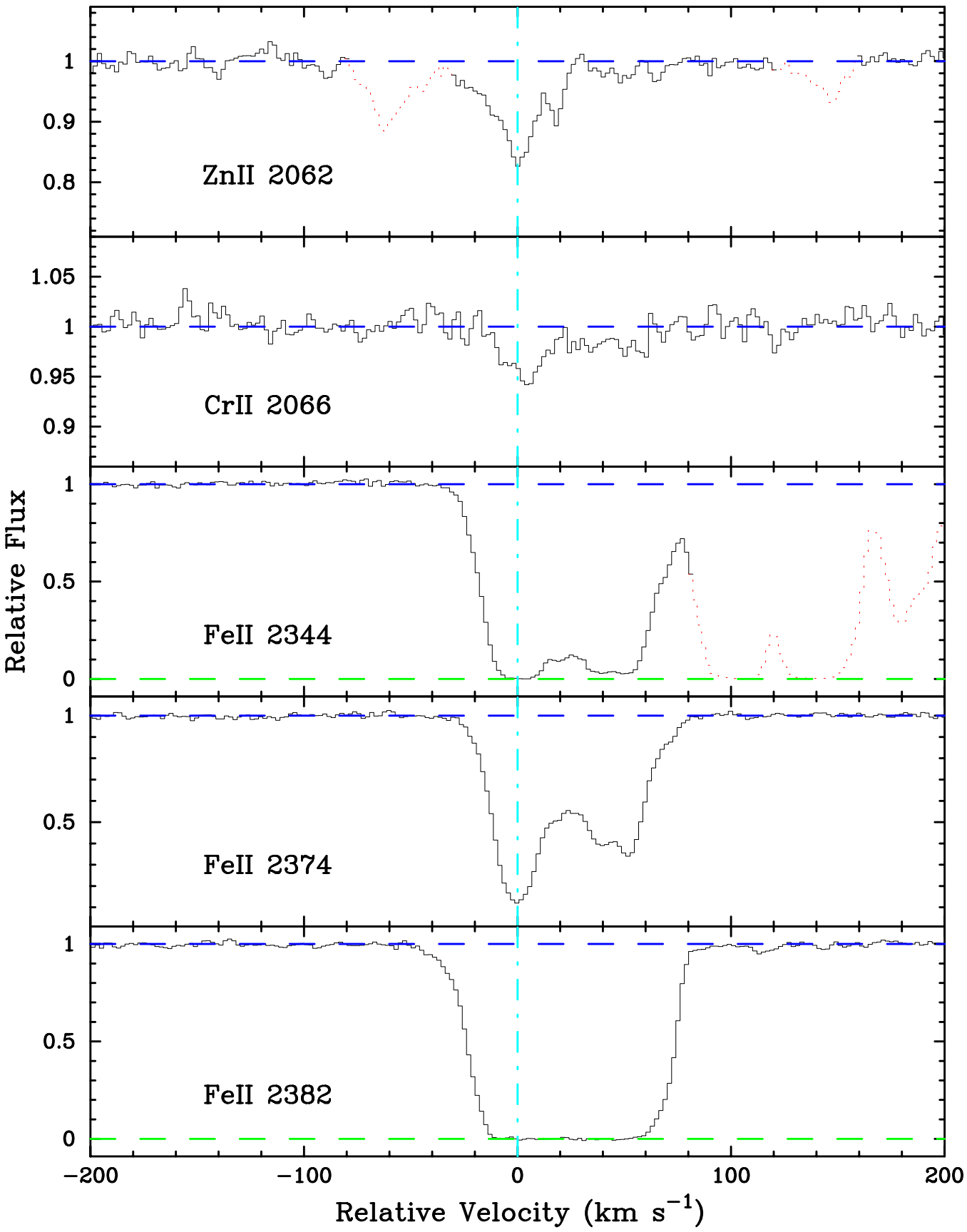

FIG. 12.—*Continued*

profiles, and unresolved in the stronger transitions even at 6 km s^{-1} resolution. This suggests that the gas in this component is at a temperature $T < 6000$ K. Although this system may be atypical because it is one of the few damped systems to exhibit C I absorption, it is worth noting that a majority of observed damped Lyα profiles may be the result of the superposition of many narrow components.

3.11. *Q1346−03*, $z = 3.736$

This very high z damped Lyα system was taken from the survey of Storrie-Lombardi et al. (1996). We present the velocity plots and column densities in Figure 13 and Table 15. We adopt log N(H I) = 20.7 ± 0.1 (Storrie-Lombardi & Wolfe 1999) throughout the analysis. Unfortunately both Fe II λ1608 and Fe II λ1611 are blended with B-band sky lines. Therefore, we have no metallicity indicator for this system and it is not included in the subsequent analysis. Measuring [Si/H] = −2.3 dex, we expect that this is a very metal poor system.

3.12. *Q1759+75*, $z = 2.625$

This system and the adopted N(H I) = 20.8 ± 0.1 are taken from an ongoing survey by I. Hook. Figure 14 presents the velocity plots, and Table 16 gives the measurements. The QSO is very bright and was observed at FWHM ≈ 6 km s^{-1} resolution. We expect that all of the measured abundances are very accurate with the exception of N(Zn$^+$) where the Zn II λ2026 profile is blended with sky lines. Although the strongest feature appears unblended, we have chosen not to include Zn in the abundance analysis.

3.13. *Q2230+02*, $z = 1.864$

Figure 15 presents the velocity plots for the damped Lyα system toward Q2230+02, and Table 17 lists the measured ionic column densities. We adopt log N(H I) = 20.85 ± 0.084 (Pettini et al. 1994) for this LBQS damped system. We have wavelength coverage of 28 metal-line transitions and have determined accurate column densities for the majority of them. This system is notable for a 4 σ detection of N(Ti$^+$). There are two Ti II transitions at 1910 Å with similar oscillator strengths and the profiles cannot be disentangled. Following the analysis presented in Prochaska & Wolfe (1997a), we integrate N_a over the entire velocity region associated with the Ti II transitions and use a reduced oscillator strength, $f^* \equiv (f_1^2 + f_2^2)/(f_1 + f_2) = 0.0862$, to calculate N(Ti$^+$). There is another difficulty in determining the Ti$^+$ column density for this system. An emission-line feature lies just blueward of the Ti II profiles and causes problems in determining the continuum level. This leads to a systematic error estimated at 0.1 dex.

The profile for the low-ion transitions is comprised of three primary features whose relative optical depth apparently varies from transition to transition. For instance, the central feature is the strongest in the Si II λ1808, Cr II λ2062, Cr II λ2066, and Zn II λ2026 profiles and the weakest in the Fe II λ2260 and Cr II λ2056 transitions. Although differences in the level of dust depletion could account for some of the variations, it would be impossible to explain the differences for a single ion (e.g., the Cr II transitions). The most likely explanation is that this central feature is a very narrow component—not fully resolved at our resolution—whose

TABLE 15

IONIC COLUMN DENSITIES: Q1346−03, $z = 3.736$

Ion	λ	AODM	$N_{\rm adopt}$	[X/H]
H I	1215	20.700 ± 0.100	...	...
C II.....	1334	14.422 ± 0.095	14.422 ± 0.095	− 2.838 ± 0.138
Al II	1670	12.546 ± 0.025	12.546 ± 0.025	− 2.634 ± 0.103
Si II	1304	13.961 ± 0.012	13.954 ± 0.011	− 2.296 ± 0.101
	1526	13.923 ± 0.026	...	...
Si IV.....	1393	12.344 ± 0.096	...	...
	1402	<12.598	...	...
Ni II.....	1370	<12.694	...	...
	1741	<13.024	...	...

TABLE 16

IONIC COLUMN DENSITIES: Q1759+75, $z = 2.625$

Ion	λ	AODM	$N_{\rm adopt}$	[X/H]
H I	1215	20.800 ± 0.100	...	...
C IV	1548	14.636 ± 0.019	...	...
	1550	14.647 ± 0.005	...	...
Al III.....	1854	13.623 ± 0.004	...	...
Si II.....	1526	>15.014	15.532 ± 0.008	− 0.818 ± 0.100
	1808	15.532 ± 0.008	...	...
Cr II	2066	13.211 ± 0.062	13.211 ± 0.062	− 1.269 ± 0.117
Fe II	1608	>14.980	15.076 ± 0.042	− 1.234 ± 0.108
	1611	15.076 ± 0.042	...	...
Ni II	1454	13.589 ± 0.039	13.565 ± 0.011	− 1.485 ± 0.101
	1709	13.615 ± 0.020	...	...
	1741	13.582 ± 0.017	...	...
	1751	13.506 ± 0.021	...	...
Zn II.....	2026	>11.650	>11.650	> −1.800

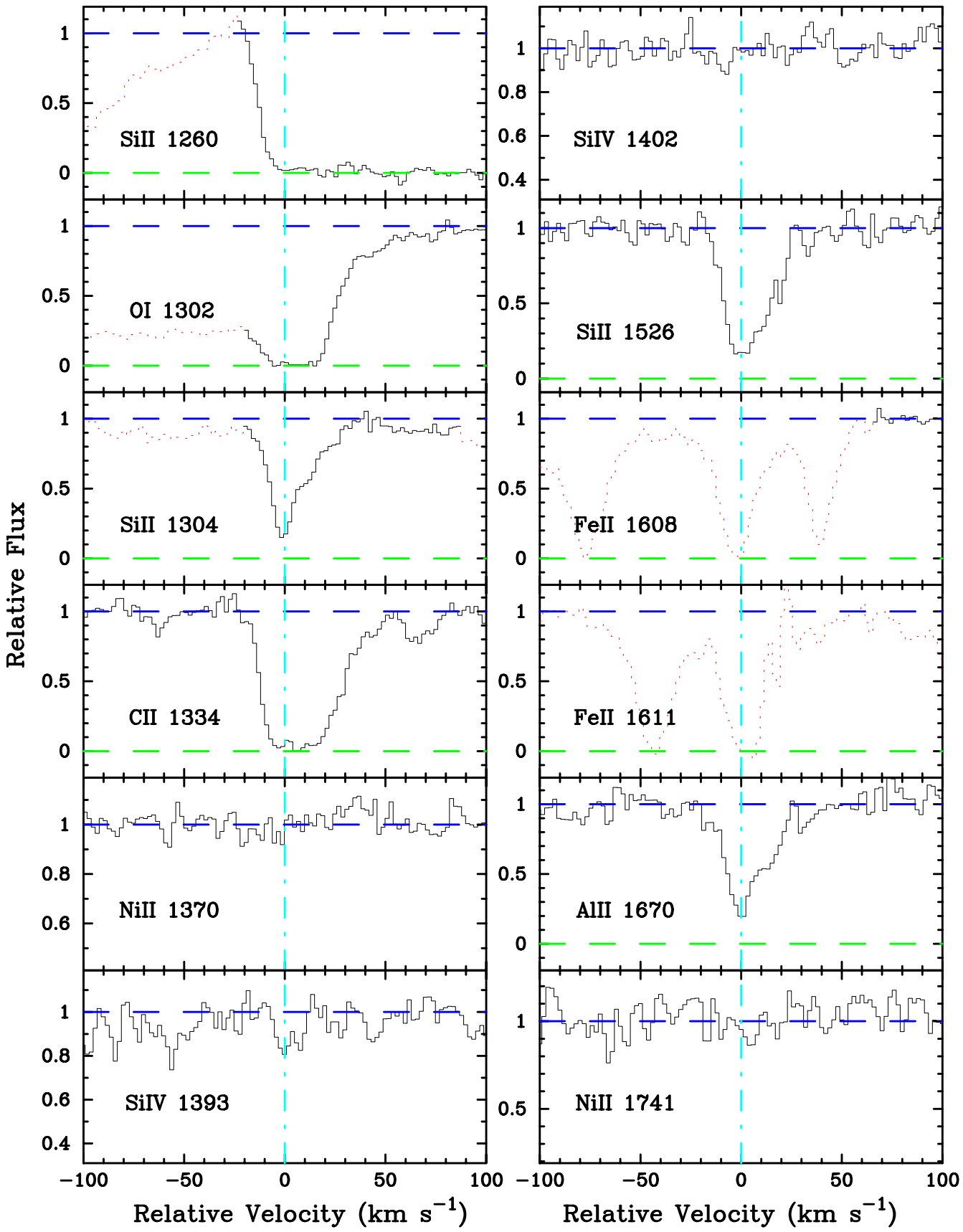

FIG. 13.—Velocity plot of the metal-line transitions for the damped Lyα system at $z = 3.736$ toward Q1346−03. The vertical line at $v = 0$ corresponds to $z = 3.735830$.

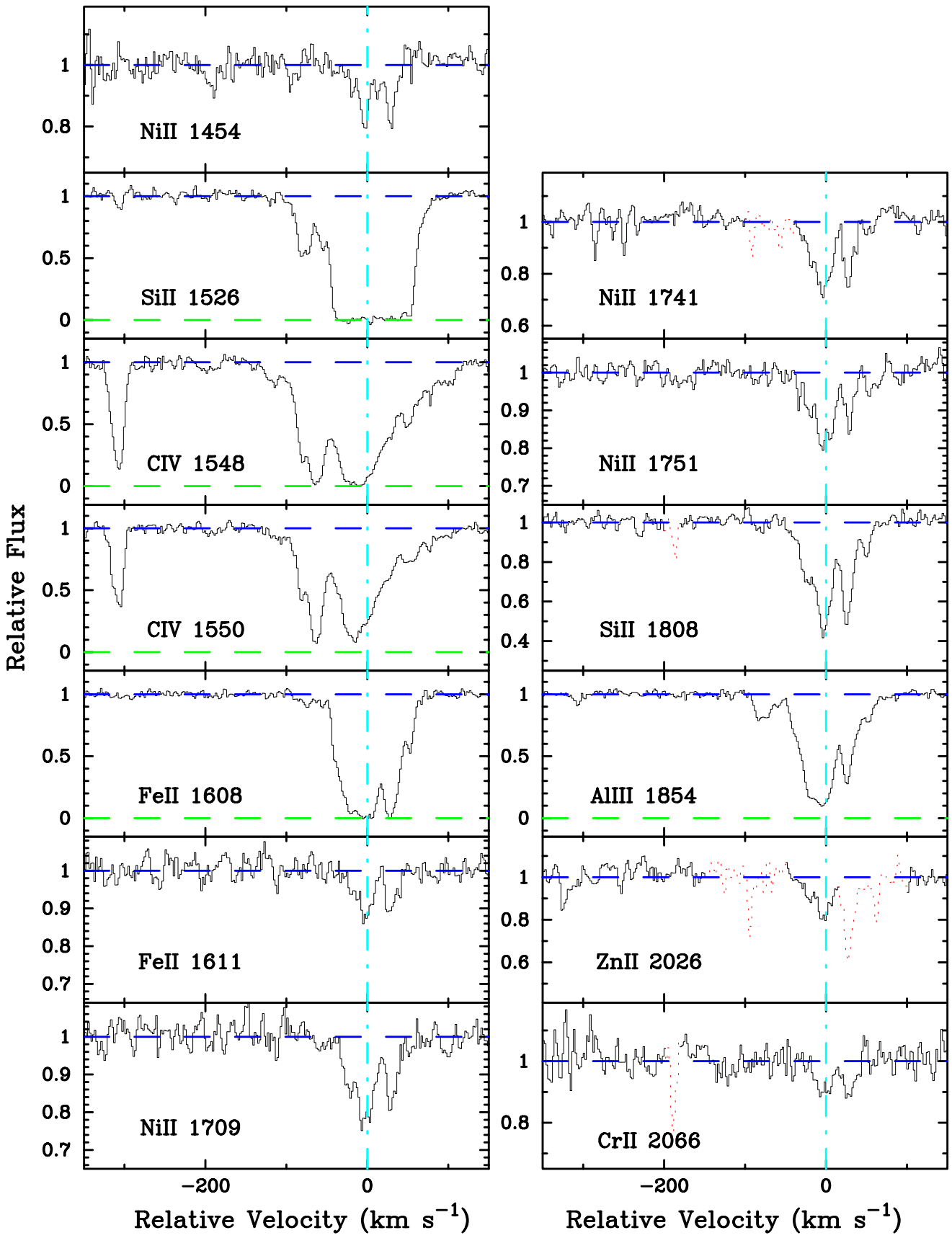

FIG. 14.—Velocity plot of the metal-line transitions for the damped Lyα system at $z = 2.625$ toward Q1759+75. The vertical line at $v = 0$ corresponds to $z = 2.6253$.

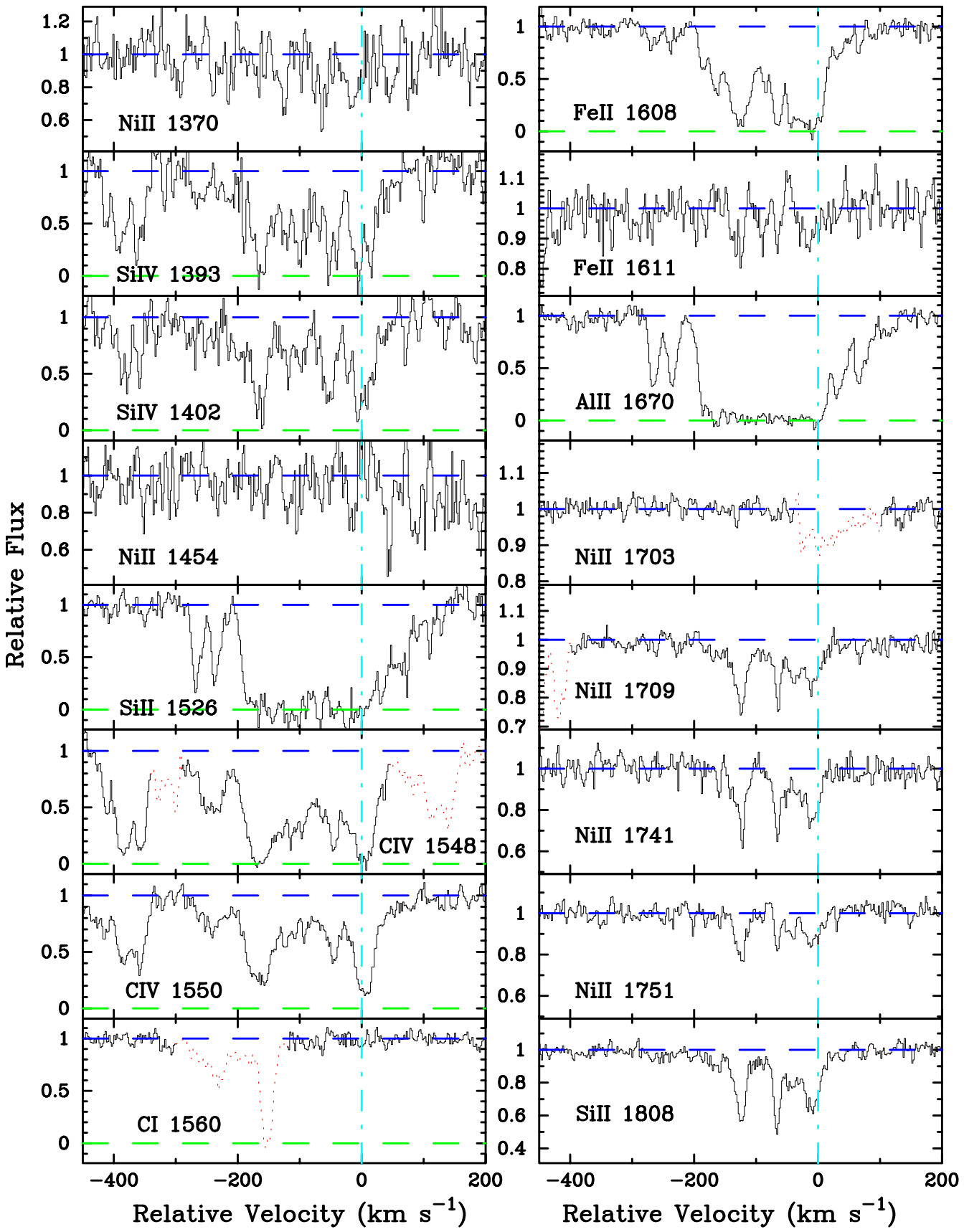

FIG. 15.—Velocity plot of the metal-line transitions for the damped Lyα system at $z = 1.864$ toward Q2230 + 02. The vertical line at $v = 0$ corresponds to $z = 1.864388$.

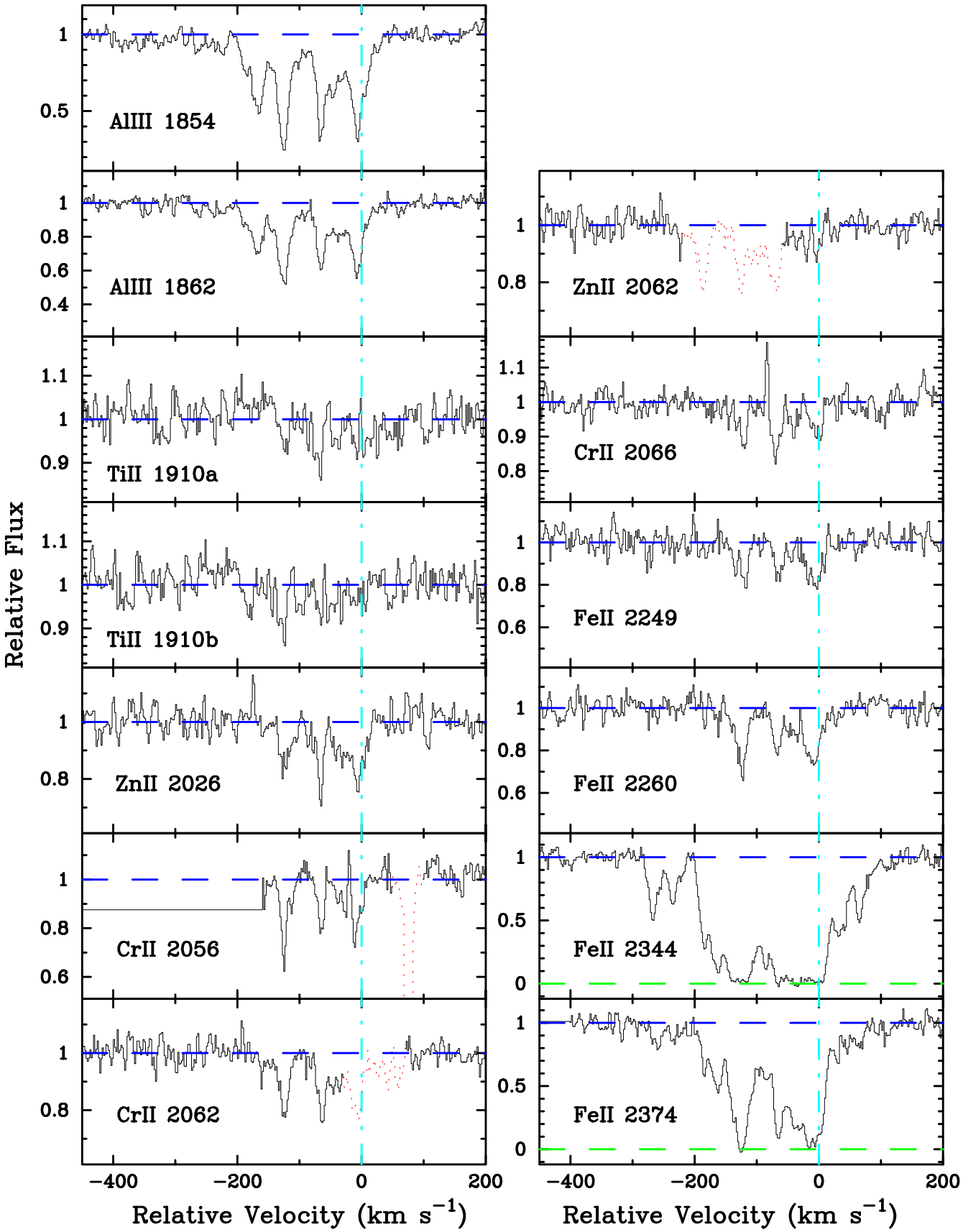

FIG. 15.—*Continued*

TABLE 17

IONIC COLUMN DENSITIES: Q2230+02, $z = 1.864$

Ion	λ	AODM	N_{adopt}	[X/H]
H I	1215	20.850 ± 0.084	...	...
C IV	1548	>14.848	...	...
	1550	14.808 ± 0.007	...	...
Al II	1670	>14.020	...	...
Al III.....	1854	13.590 ± 0.006	...	...
	1862	13.596 ± 0.009	...	...
Si II.....	1526	>15.233	15.656 ± 0.010	-0.744 ± 0.085
	1808	15.656 ± 0.010	...	...
Si IV	1393	>14.267	...	...
	1402	>14.354	...	...
Ti II	1910	12.985 ± 0.099	12.985 ± 0.099	-0.795 ± 0.130
Cr II	2056	13.361 ± 0.036	13.403 ± 0.027	-1.127 ± 0.088
	2066	13.483 ± 0.041	...	...
Fe II	1608	>15.115	15.188 ± 0.016	-1.172 ± 0.086
	1611	15.273 ± 0.084	...	...
	2249	15.120 ± 0.036	...	...
	2260	15.210 ± 0.019	...	...
	2344	>14.988	...	...
	2374	>15.183	...	...
	2382	>14.723	...	...
Ni II	1370	13.883 ± 0.052	13.812 ± 0.011	-1.288 ± 0.085
	1709	13.860 ± 0.014	...	...
	1741	13.838 ± 0.023	...	...
	1751	13.687 ± 0.028	...	...
Zn II.....	2026	12.800 ± 0.028	12.800 ± 0.028	-0.700 ± 0.088

relative optical depth varies significantly with the strength of the transition. Finally, this system is notable for the presence of a nearby metal-line system at ≈ -550 km s^{-1}, which shows multiple metal transitions (Fig. 16). The subsystem exhibits ionic column densities typical of a damped Lyα system and its $Al^+/Al^{++} = 2.6$ ratio indicates that the system is nearly neutral. Therefore, it is almost certainly contributing to the measured N(H I) for this system, which would mean that we are underestimating the metallicity of the system at $z = 1.864$. Because the nearby system exhibits ionic column densities at less than 10% of the damped system, we have chosen to ignore its effects in our abundance analysis.

3.14. *Q2231−00*, $z = 2.066$

This LBQS system is another damped Lyα system exhibiting significant (5 σ) Ti II λ1910 absorption. As in the damped Lyα system toward Q2230+02, the Ti II profiles overlap, hence we use the technique outlined above to determine $N(Ti^+)$. Throughout the analysis we adopt log N(H I) = 20.56 ± 0.1 (Pettini et al. 1994). The velocity plots are given in Figure 17, and the column densities are presented in Table 18. This is the other system in our data sample that was previously observed by Lu et al. (1996). We find our measurements match theirs in nearly every case, although their analysis did not include Ti^+.

3.15. *Q2348−14*, $z = 2.279$

This very metal poor system was first discussed by Pettini et al. (1994) and has been previously observed at high resolution by Pettini, Lipman, & Hunstead (1995). The velocity plots are given in Figure 18, and Table 19 lists the measured ionic column densities for this system. In Figure 19 we plot the Lyα transition for this system. Overplotted are Voigt profiles centered at $z = 2.2794$ with log N(H I) = 20.56 ± 0.075 corresponding to the measurements made by Pettini et al. (1994). Although the profiles provide a reasonable fit to the left wing of the damped profile, the fit for $v > 750$ km s^{-1} is clearly inconsistent for all of the assumed N(H I) values. It is very difficult, however, to continuum fit an order of HIRES data that includes a damped Lyα profile; it is easier to fit intermediate resolution data. Therefore, we adopt log N(H I) = 20.56 ± 0.075 from the Pettini et al. analysis but note in passing that this may be an overestimate of the true N(H I) value. Comparing our derived chemical abundances with the work of Pettini et al. (1995), we find reasonable agreement and note that we have improved on their limits in a few cases (e.g., N and S).

The system is exceptional for a number of reasons. First, it is one of the few systems where we have a measurement of $N(S^+)$ based on the S II λ1259 transition. As discussed for the damped system toward Q0347−38, S/Fe is an excellent diagnostic of dust depletion. Here we find [S/FeFe] = 0.17 dex, which argues strongly against dust depletion *if* the system has an underlying Type II SN pattern. Second, the system exhibits two distinct low-ion features, one at $v \approx -100$ km s^{-1} (feature 1; this feature was not resolved in previous observations) and the more dominant at $v \approx 0$ km s^{-1} (feature 2). Feature 1 is present in all of the Si II transitions and is the strongest feature in the Al III, C IV, and Si IV profiles. Comparing $N(Si^+)$ for the two features in the Si II λ1526 profile, we find $N(Si^+)_1/N(Si^+)_2 = 0.18$. At the same time, however, the feature is entirely absent in the O I λ1302 and Fe II λ1608 profiles: $N(O^0)_1/N(O^0)_2 < 0.027$ and $N(Fe^+)_1/N(Fe^+)_2 < 0.07$. Although dust could possibly explain the absence of Fe where Si is present because Si is only lightly depleted in the ISM, it cannot account for the lack of O I absorption. The system corresponding to feature 1 must be significantly ionized such that the dominant

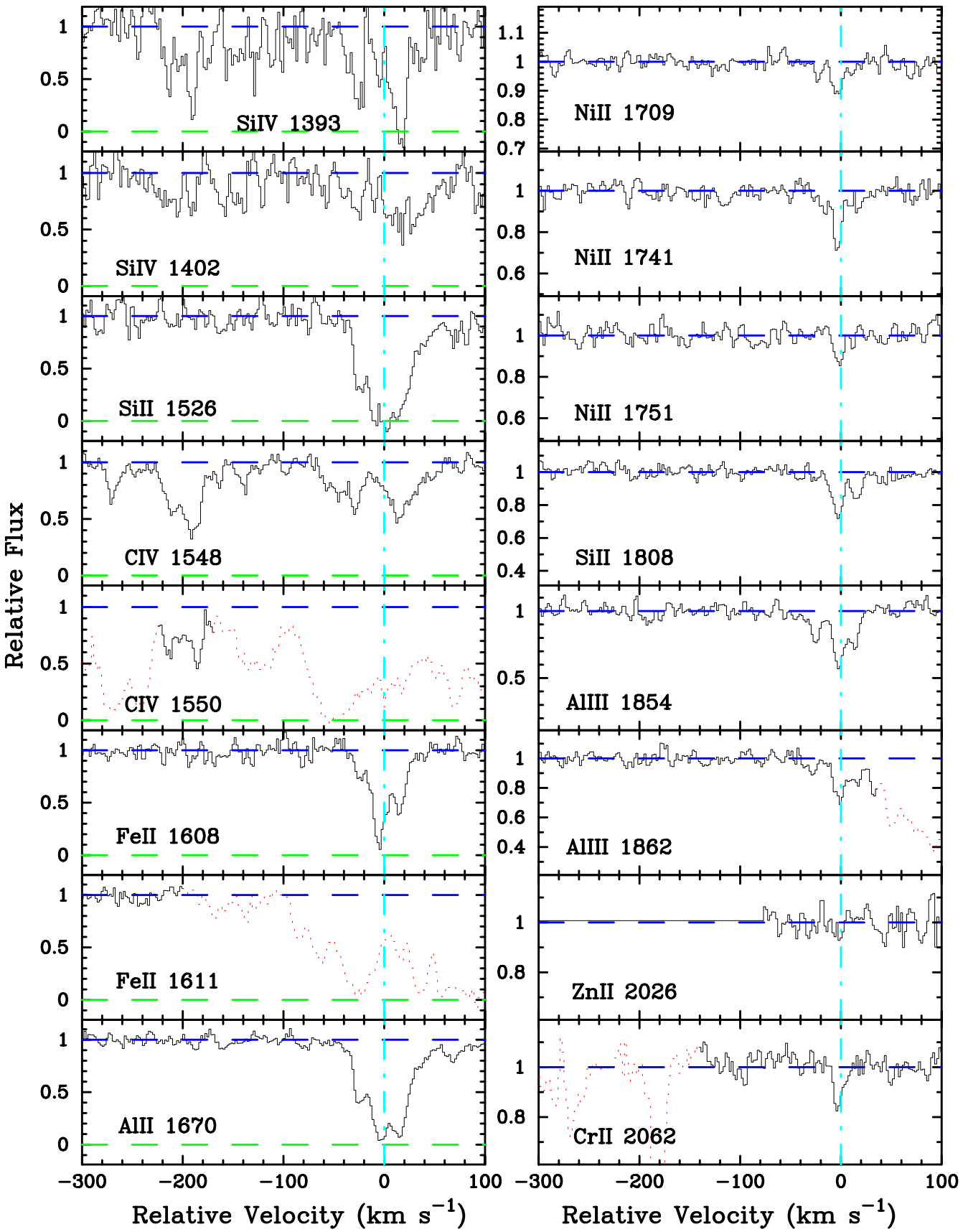

FIG. 16.—Velocity plot of the metal-line transitions for the presumed damped system at $z = 1.859$ toward Q2230 + 02. The vertical line at $v = 0$ corresponds to $z = 1.858536$.

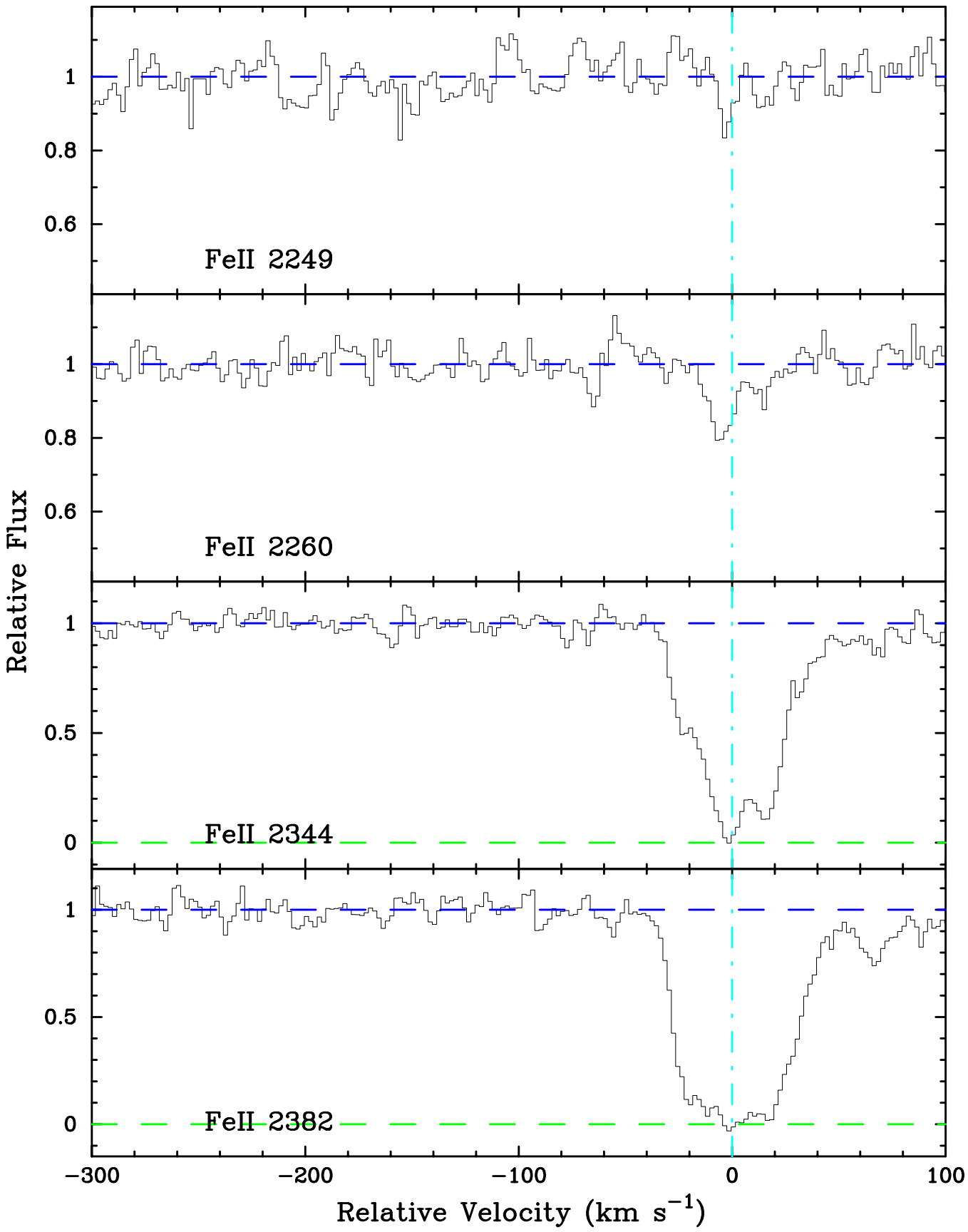

FIG. 16.—*Continued*

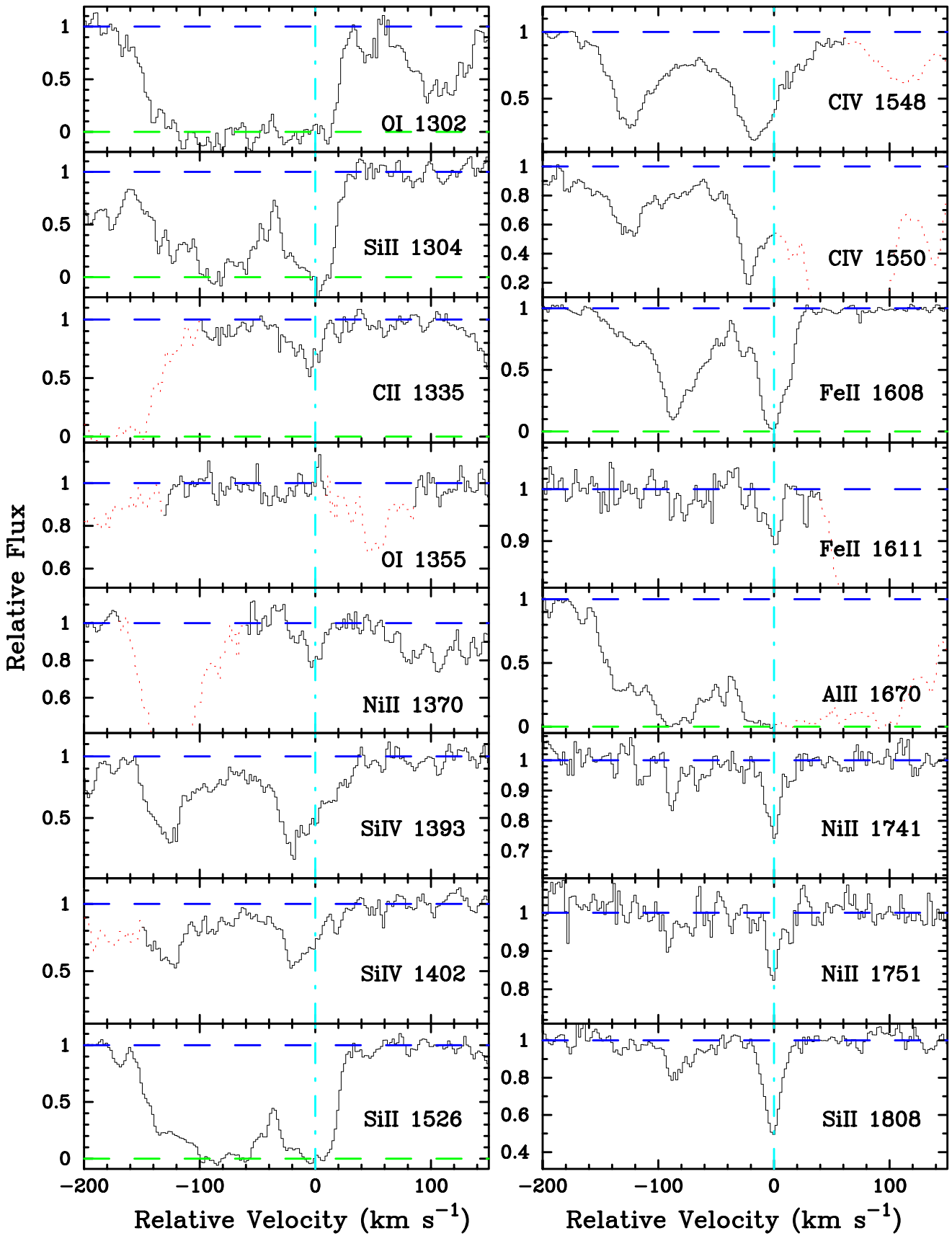

FIG. 17.—Velocity plot of the metal-line transitions for the damped Lyα system at $z = 2.066$ toward Q2231 − 00. The vertical line at $v = 0$ corresponds to $z = 2.06615$.

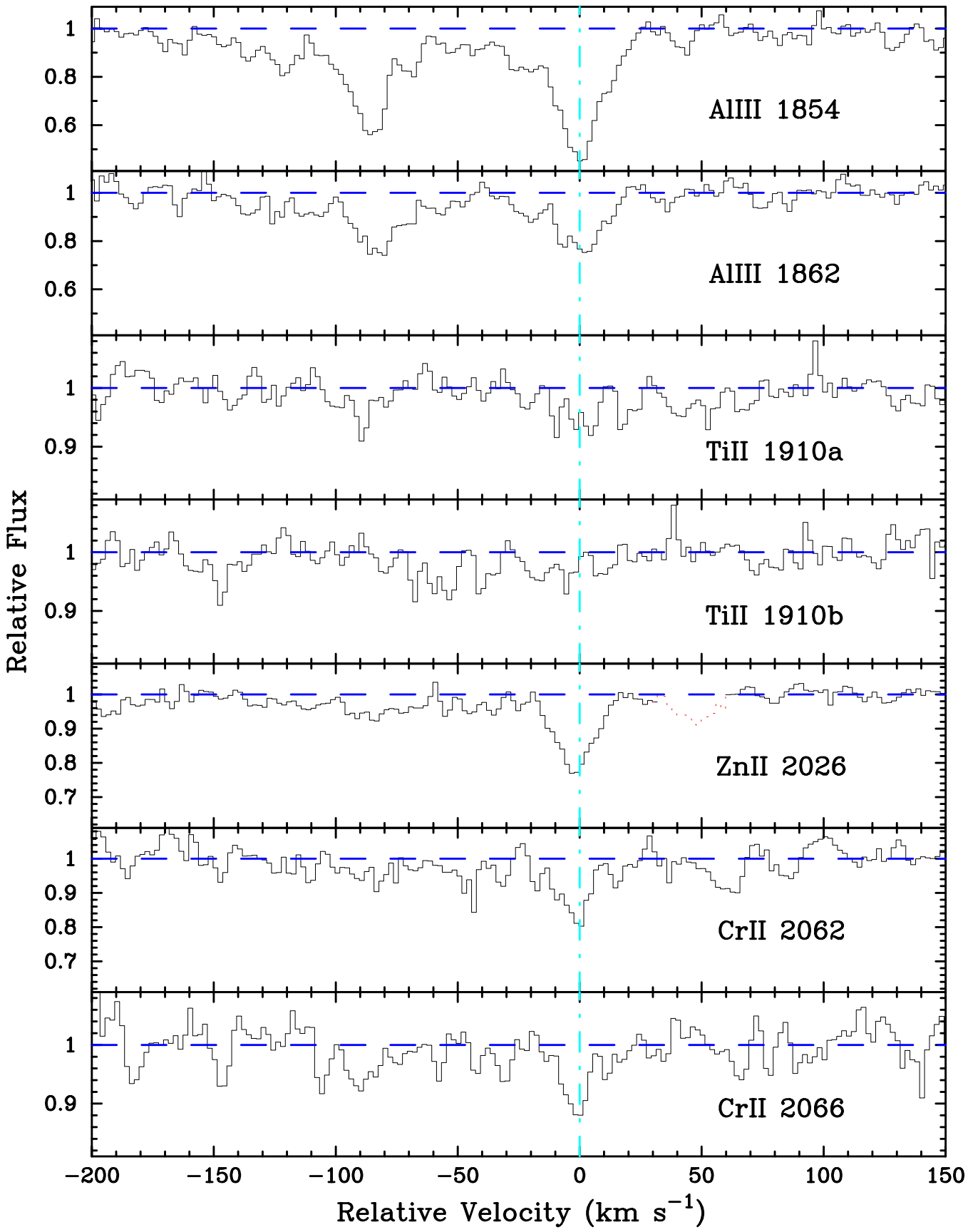

FIG. 17.—*Continued*

TABLE 18

IONIC COLUMN DENSITIES: Q2231−00, $z = 2.066$

Ion	λ	AODM	N_{adopt}	[X/H]
H I	1215	20.560 ± 0.100	...	...
C II	1335	13.580 ± 0.040	...	...
C IV	1548	14.195 ± 0.005	...	...
O I	1302	>15.543	<17.748	<0.258
	1355	<17.748	...	...
Al III.....	1854	13.172 ± 0.010	...	...
	1862	13.110 ± 0.023	...	...
Si II.....	1304	>15.030	15.247 ± 0.019	-0.863 ± 0.102
	1526	>15.014	...	...
	1808	15.247 ± 0.019	...	...
Si IV	1393	13.704 ± 0.010	...	...
	1402	13.698 ± 0.012	...	...
Ti II	1910	12.848 ± 0.071	12.848 ± 0.071	-0.642 ± 0.123
Cr II	2062	13.182 ± 0.040	13.165 ± 0.034	-1.075 ± 0.106
	2066	13.130 ± 0.063	...	...
Fe II	1608	14.750 ± 0.009	14.750 ± 0.009	-1.320 ± 0.100
	1611	14.783 ± 0.065	...	...
Ni II	1370	12.880 ± 0.091	13.306 ± 0.032	-1.504 ± 0.105
	1741	13.381 ± 0.033	...	...
	1751	13.100 ± 0.091	...	...
Zn II.....	2026	12.463 ± 0.023	12.463 ± 0.023	-0.747 ± 0.103

states of O, Fe, and Si are higher ions. We have performed CLOUDY (Ferland 1991) calculations that demonstrate that values of $[Si^+/O^0] \approx 1.2$ dex and $[Si^+/Fe^+] \approx 0.7$ dex are possible in a Lyman limit system provided the ionization parameter is significantly high. Therefore, we argue that feature 2 marks the damped Lyα system, whereas feature 1 may be a significantly ionized satellite or halo cloud. The system is also notable for providing a meaningful estimate of N/O. Finally, perhaps the most remarkable characteristic of this damped system is the velocity width of the C IV profiles, $\Delta v > 600$ km s^{-1}, particularly in light of the very narrow Δv exhibited by the low-ion profiles. This kinematic observation poses a difficult challenge to any physical model introduced to explain the damped Lyα systems.

3.16. *Q2359−02, $z = 2.095$ and $=2.154$*

This faint QSO exhibits two intervening damped Lyα systems. Both are members of the LBQS statistical survey. The velocity plots and column densities for the $z = 2.095$ system are presented in Figure 20 and Table 20, and those for the $z = 2.154$ are given by Figure 21 and Table 21. Both are part of the LBQS statistical sample, and we have taken the H I column densities from Wolfe et al. (1995): log N(H I) $= 20.7 \pm 0.1$ for the $z = 2.095$ system and log N(H I) $= 20.3 \pm 0.1$ for the $z = 2.154$ system. The S/N is relatively low for most of the spectrum, and therefore abundances established on the weakest transitions are suspect, particularly those for Zn. We intend to make further observations of these two systems to improve the accuracy of our abundance measurements.

4. ABUNDANCE PATTERNS

Table 22 lists the relative logarithmic abundances for the damped Lyα systems, $[X/H] \equiv \log [N(X)/N(H)] - \log [N(X)/N(H)]_\odot$. For each system we adopt the value

TABLE 19

IONIC COLUMN DENSITIES: Q2348−14, $z = 2.279$

Ion	λ	AODM	N_{adopt}	[X/H]
H I	1215	20.560 ± 0.075	...	...
C II	1334	>14.610	...	...
	1335	13.207 ± 0.070	...	...
N I	1200	<13.223	<13.223	<-3.387
O I	1302	>14.798	>14.798	>-2.692
Al II	1670	12.654 ± 0.006	12.654 ± 0.006	-2.386 ± 0.075
Al III.....	1854	12.726 ± 0.012	...	...
	1862	12.613 ± 0.027	...	...
Si II.....	1190	>14.207	14.201 ± 0.010	-1.909 ± 0.076
	1193	>13.924	...	...
	1260	>13.744	...	...
	1304	14.227 ± 0.021	...	...
	1526	14.201 ± 0.011	...	...
	1808	14.089 ± 0.059	...	...
Si IV	1393	>14.063	...	...
S II	1259	13.725 ± 0.119	13.725 ± 0.119	-2.105 ± 0.140
Fe II	1608	13.792 ± 0.016	13.792 ± 0.016	-2.278 ± 0.077

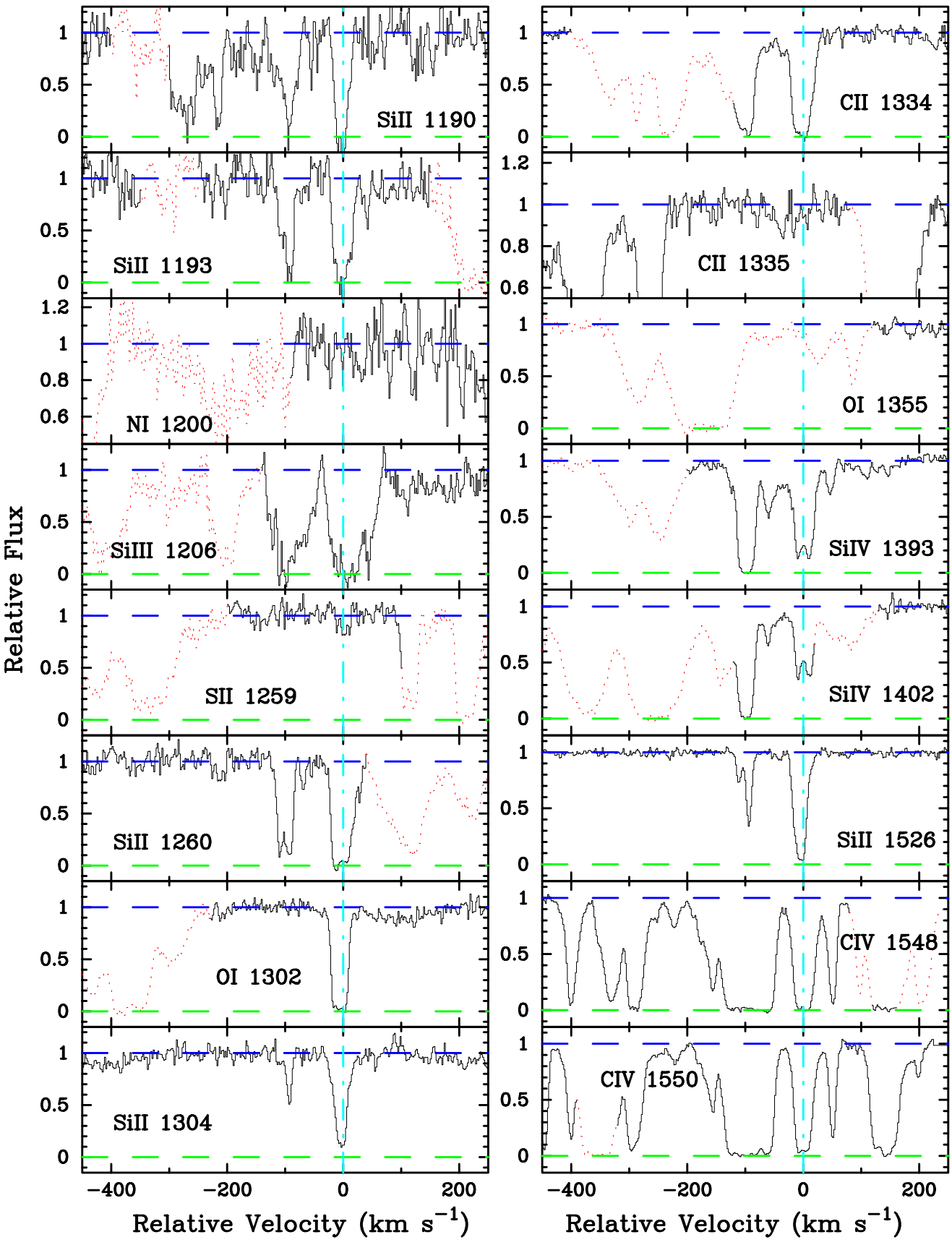

FIG. 18.—Velocity plot of the metal-line transitions for the damped Lyα system at $z = 2.279$ toward Q2348 − 14. The vertical line at $v = 0$ corresponds to $z = 2.2794$.

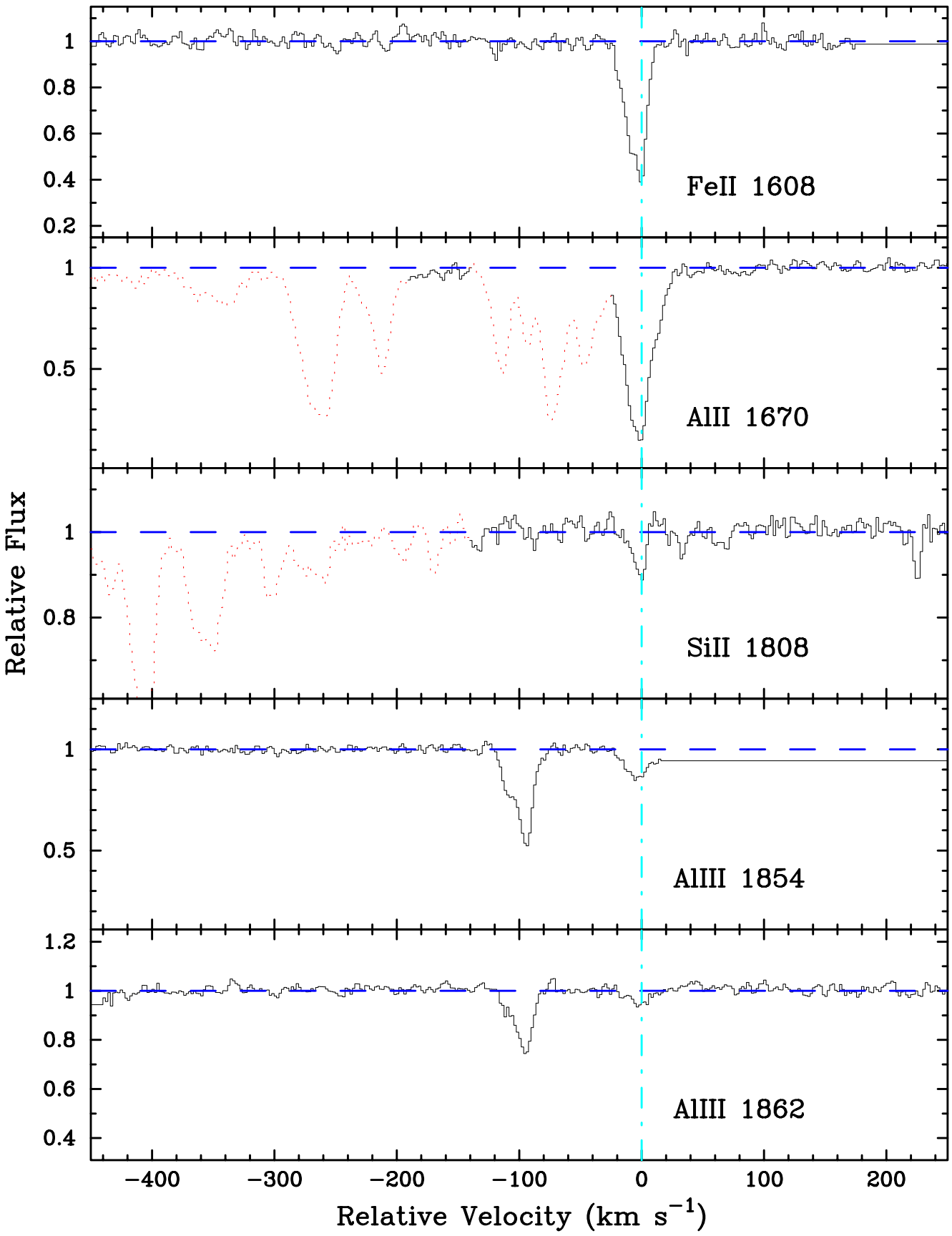

FIG. 18.—*Continued*

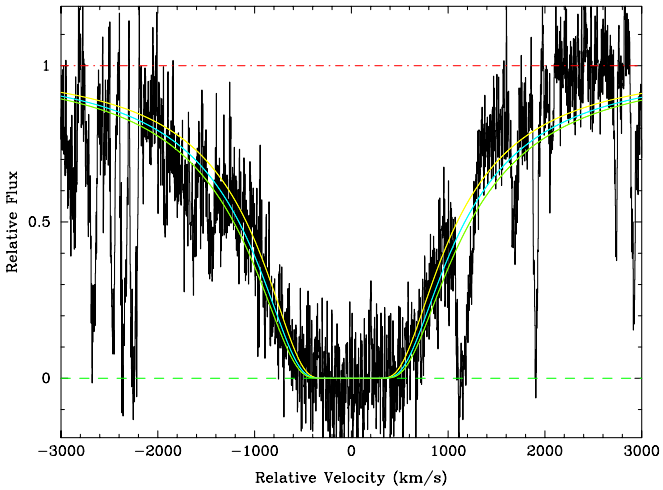

FIG. 19.—Lyα profile for the damped system toward Q2348−14. The overplotted curves correspond to $N(\mathrm{H\ I}) = 20.56 \pm 0.075$.

for N(H I) indicated in the previous section and calculate N(X) by performing a weighted mean of all direct measurements, i.e., no limits or blends. Included in Table 22 are the abundance measurements for the damped Lyα systems toward Q0201+36 and Q2206−19. In a few cases the values differ from the published values in light of new oscillator strengths. It is well established both observationally and theoretically that the damped Lyα systems are primarily neutral (Viegas 1994; Prochaska & Wolfe 1996). Therefore we perform no ionization corrections in determining the abundances from the ionic column densities of the low ions.

Figure 22 presents the abundance patterns for the most common elements in our full sample. We have chosen not to include error bars for presentation purposes; the derived errors are less than 0.1 dex with only a few exceptions. Following Lu et al. (1996), along the x-axis of each panel we plot metallicity—here expressed with [Fe/H]—in part because this is the primary metallicity indicator in local stellar populations and in part because we have Fe abundance measurements for a greater number of systems. Examining the upper left panel of Figure 22, we note a systematic overabundance of Zn/Fe, which suggests that Fe may be depleted onto dust grains. Therefore consider the [Fe/H] values to be lower limits to the true metallicity. In one case (Q0841+12A) we have no reliable Fe abundance measurement and have taken [Fe/H] = [Cr/H] on the grounds that [Cr/H] ≈ [Fe/H] in the majority of damped Lyα systems.

In the following, we discuss the evidence for dust depletion and Type II supernova enrichment in light of the observed damped Lyα abundance patterns. The former is determined by comparing against abundance patterns in depleted ISM clouds (Savage & Sembach 1996), whereas the latter is assessed by comparing against the abundance patterns of metal-poor halo stars presumed to exhibit

TABLE 20

IONIC COLUMN DENSITIES: Q2359−02, $z = 2.095$

Ion	λ	AODM	N_{adopt}	[X/H]
H I	1215	20.700 ± 0.100	...	...
C II	1334	>15.146	...	...
C IV	1548	>14.639	...	...
	1550	>14.800	...	...
Al II	1670	13.662 ± 0.034	13.662 ± 0.034	−1.518 ± 0.106
Al III.....	1854	13.383 ± 0.010	...	...
	1862	13.396 ± 0.016	...	...
Si II.....	1526	>15.045	15.408 ± 0.021	−0.842 ± 0.102
	1808	15.408 ± 0.021	...	...
Si IV	1393	>14.072	...	...
	1402	>14.517	...	...
Cr II	2056	12.748 ± 0.091	12.748 ± 0.091	−1.632 ± 0.135
	2062	13.131 ± 0.057	...	...
	2066	<12.897	...	...
Fe II	1608	14.507 ± 0.025	14.507 ± 0.025	−1.703 ± 0.103
	1611	<15.077	...	...
Ni II	1703	<13.693	13.142 ± 0.054	−1.808 ± 0.114
	1709	13.152 ± 0.127	...	...
	1741	13.185 ± 0.072	...	...
	1751	13.071 ± 0.107	...	...
Zn II.....	2026	12.595 ± 0.029	12.595 ± 0.029	−0.755 ± 0.104
	2062	12.486 ± 0.075	...	...

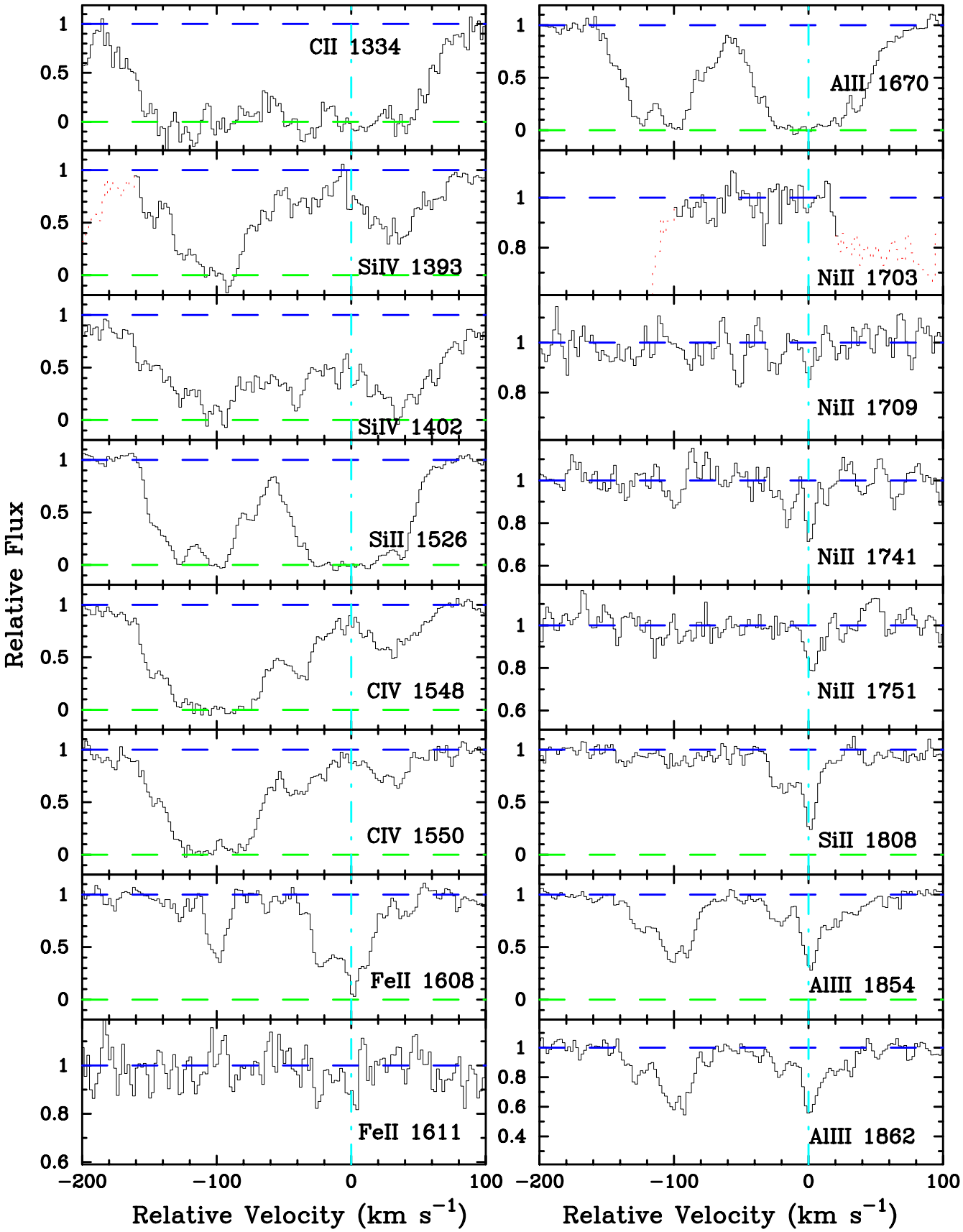

FIG. 20.—Velocity plot of the metal-line transitions for the damped Lyα system at $z = 2.095$ toward Q2359 − 02. The vertical line at $v = 0$ corresponds to $z = 2.095067$.

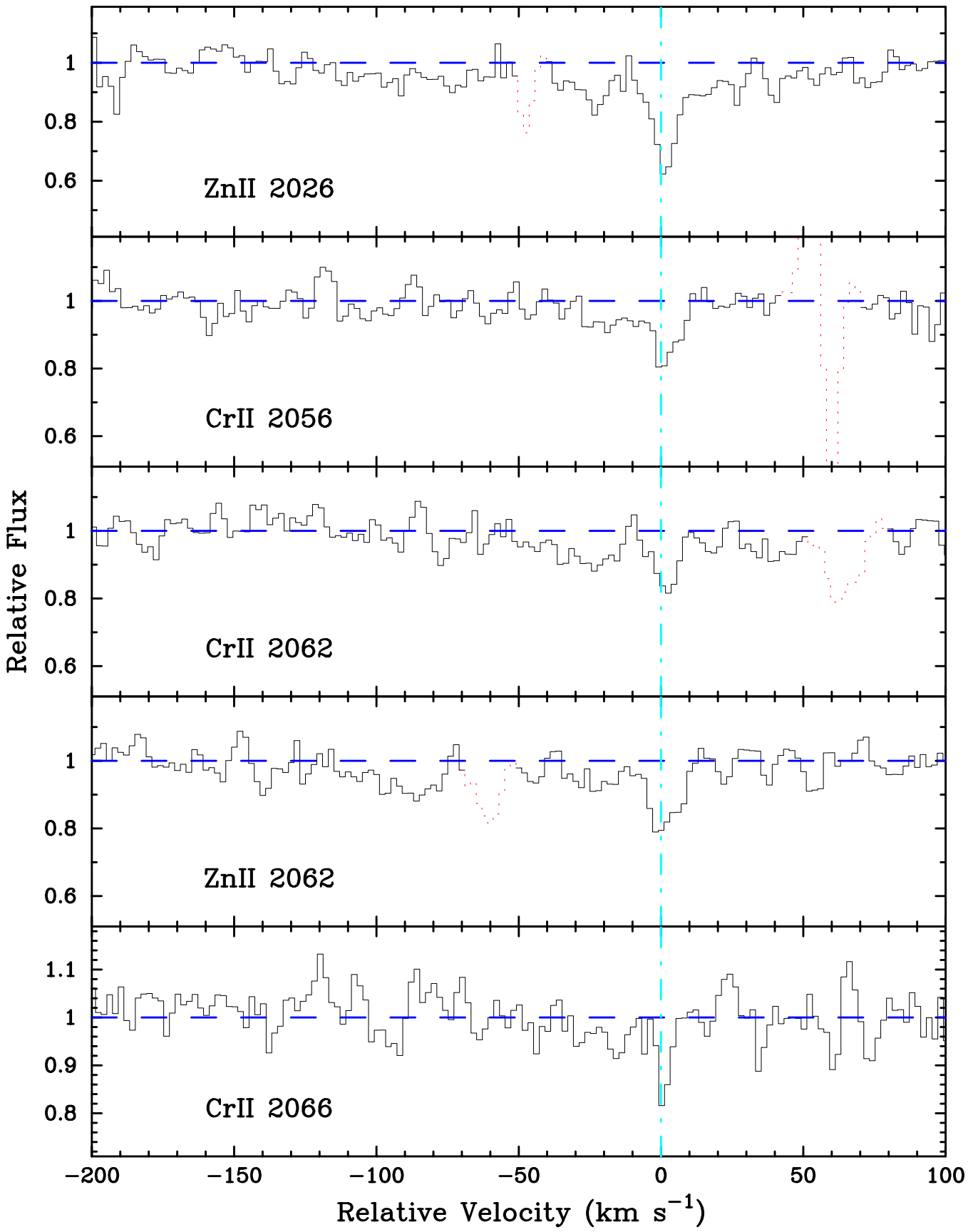

FIG. 20.—*Continued*

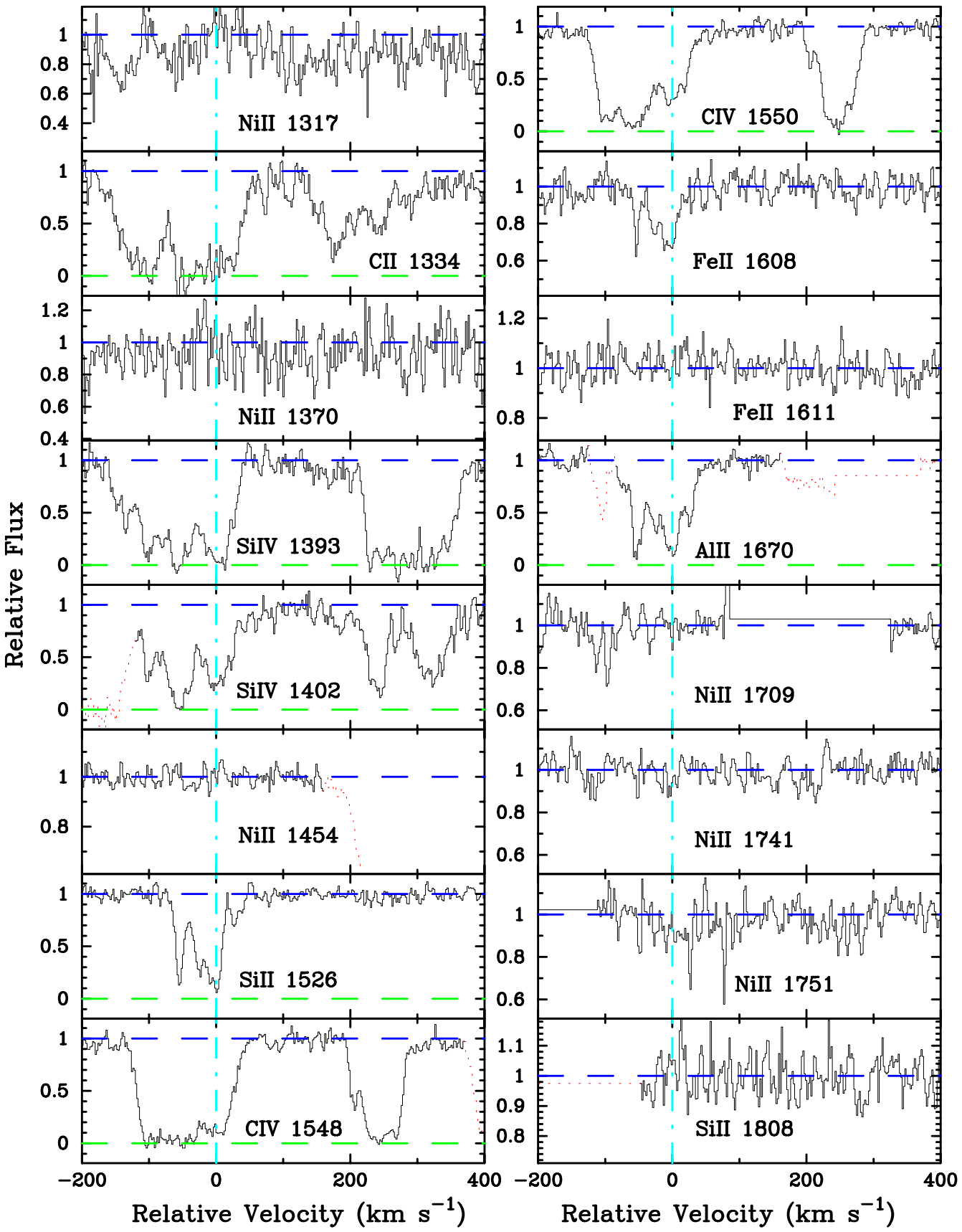

FIG. 21.—Velocity plot of the metal-line transitions for the damped Lyα system at $z = 2.154$ toward Q2359 − 02. The vertical line at $v = 0$ corresponds to $z = 2.153934$.

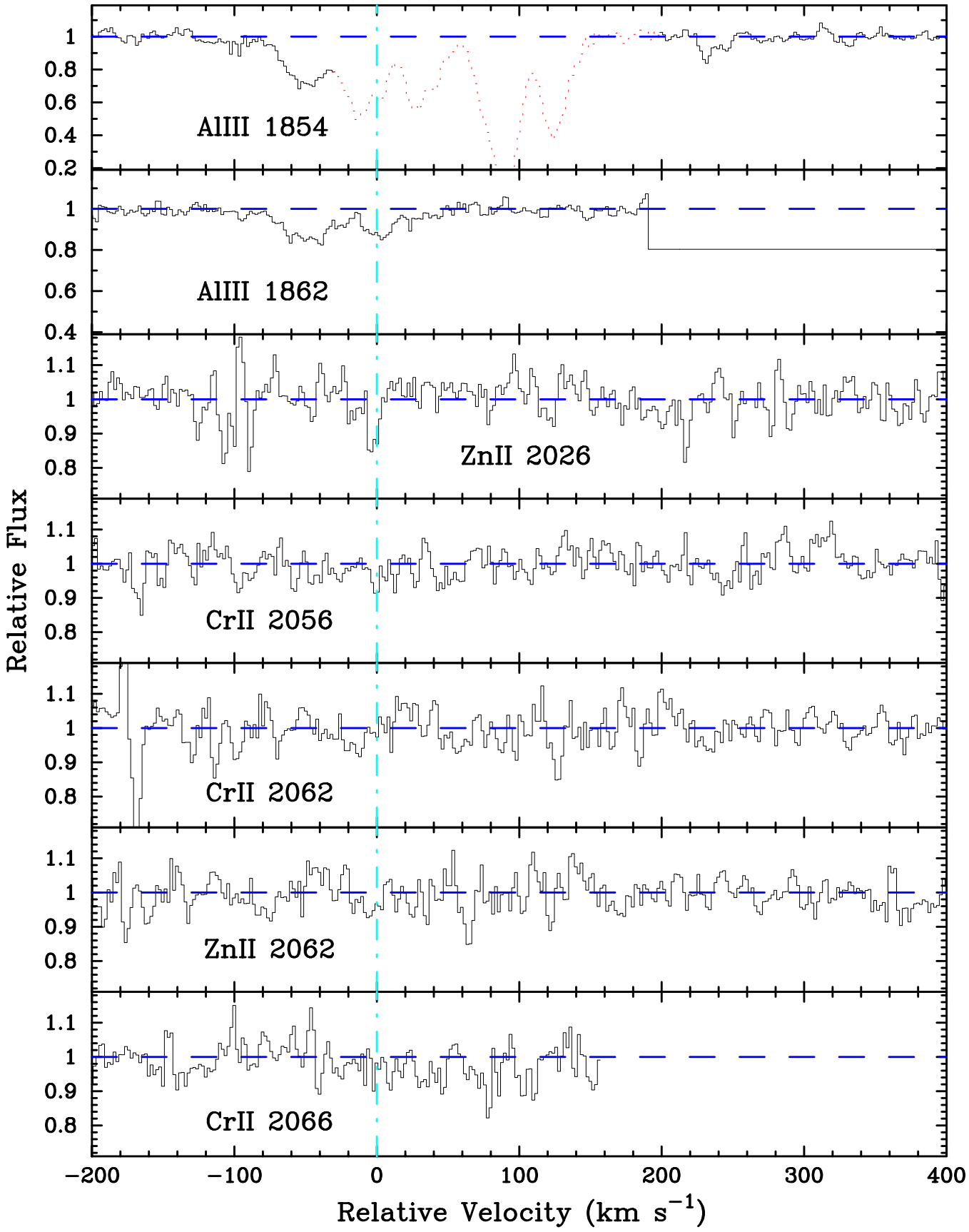

FIG. 21.—*Continued*

TABLE 21

IONIC COLUMN DENSITIES: Q2359−02, $z = 2.154$

Ion	λ	AODM	$N_{\rm adopt}$	[X/H]
H I	1215	20.300 ± 0.100	...	...
C II	1334	>14.987	...	...
C IV	1548	>14.880	...	...
	1550	>14.966	...	...
Al II	1670	13.165 ± 0.016	13.165 ± 0.016	-1.615 ± 0.101
Al III.....	1862	12.960 ± 0.021	...	...
Si II.....	1526	14.316 ± 0.015	14.316 ± 0.015	-1.534 ± 0.101
Si IV	1393	>14.568	...	...
	1402	>14.528	...	...
Cr II	2056	<12.549	<12.946	<-1.034
	2066	<12.946	...	...
Fe II	1608	13.895 ± 0.032	13.895 ± 0.032	-1.915 ± 0.105
	1611	<14.917	...	...
Ni II	1317	<13.152	<12.949	<-1.601
	1370	<13.248	...	...
	1454	<13.063	...	...
	1741	<12.949	...	...
	1751	<13.200	...	...
Zn II.....	2026	<11.901	<11.901	<-1.049

nucleosynthetic patterns typical of Type II supernovae (McWilliam 1997). First, consider the top two panels of Figure 22, which lend support to the presence of significant dust depletion in the damped Lyα systems. As described throughout the paper, the overabundance of Zn to Fe relative to solar abundances is suggestive of dust depletion both because (1) Zn is largely undepleted in dusty regions within the ISM whereas Fe is heavily depleted and (2) [Zn/Fe] ≈ 0 dex for stars of all metallicity observed within the Galaxy (Sneden, Gratton, & Crocker 1991). Similarly, the Ni/Fe ratio is significantly lower than metal-poor halo stars, which is consistent with Ni being more heavily depleted than Fe in depleted regions of the ISM. Lu et al. (1996) have argued that the underabundance is primarily due to an error in the oscillator strengths for the Ni II transitions. Although a recent analysis by Zsargó & Federman (1998) indicates that the Ni II f values are poorly determined, it is not clear whether this can entirely account for the discrepancy between the damped Lyα observations and the metal-poor halo star abundances. For our analysis, we have adopted the updated f values from Zsargó & Federman (1998)—which does include a decrease in f_{1714} by a factor of 1.34—yet a significant underabundance of [Ni/Fe] is still apparent. Therefore it is unclear whether errors in the oscillator strengths can fully resolve the discrepancy between the observed Ni/Fe pattern and that predicted for Type II SN yields.

In contrast to the top two panels, the middle panels and the Al/Fe abundance pattern are generally consistent with both dust depletion and Type II SN enrichment. As empha-

TABLE 22

ABUNDANCES

DLA	$z_{\rm abs}$	log [N(H I)]	[Si/H]	[Al/H]	[S/H]	[Fe/H]	[Ni/H]	[Cr/H]	[Zn/H]
Q0000−26.....	3.390	21.410	−1.874	...	...	−1.774	−2.335	...	...
Q0019−01.....	3.439	20.900	−1.027	...	...	−1.640	−1.708	...	...
Q0100+13.....	2.309	21.400	>-2.228	...	...	−1.814	−2.030	−1.693	−1.556
Q0149+33.....	2.141	20.500	−1.683	−2.044	...	−1.808	−1.850	−1.369	−1.654
Q0201+36.....	2.463	20.380	−0.376	...	...	−0.878	−0.877	−0.776	−0.266
Q0347−38.....	3.025	20.800	−1.530	...	−1.339	−1.838	<-2.373	...	...
Q0458−02.....	2.040	21.650	>-2.105	...	...	−1.652	−2.047	−1.533	−1.159
Q0841+12A.....	2.375	20.950	−1.261	>-2.163	...	...	−1.957	−1.551	−1.485
Q0841+12B.....	2.476	20.780	>-1.869	−2.074	...	−1.856	−1.982	−1.620	<-1.652
Q0951−04A.....	3.857	20.600	−1.505	−1.782	...	−2.048	−1.856	...	...
Q0951−04B.....	4.203	20.400	−2.558	...	...	<-2.629	<-2.061	...	...
Q1215+33.....	1.999	20.950	−1.470	...	...	−1.812	−1.856	−1.500	−1.309
Q1331+17.....	1.776	21.176	−1.441	...	...	−2.088	−2.191	−1.937	−1.221
Q1346−03.....	3.736	20.700	−2.296	−2.634	...	...	...	...	...
Q1759+75.....	2.625	20.800	−0.818	...	...	−1.234	−1.485	−1.269	>-1.800
Q2206−19A.....	1.920	20.653	−0.402	...	...	−0.705	−0.903	−0.580	−0.379
Q2206−19B.....	2.076	20.431	−2.225	−2.727	...	−2.621	<-2.38	<-2.00	<-1.745
Q2230+02.....	1.864	20.850	−0.744	...	...	−1.172	−1.288	−1.127	−0.700
Q2231−00.....	2.066	20.560	−0.863	...	...	−1.320	−1.504	−1.075	−0.747
Q2348−14.....	2.279	20.560	−1.909	−2.386	−2.105	−2.278	...	...	...
Q2359−02A.....	2.095	20.700	−0.842	−1.518	...	−1.703	−1.808	−1.632	−0.755
Q2359−02B.....	2.154	20.300	−1.534	−1.615	...	−1.915	<-1.601	<-1.034	<-1.049

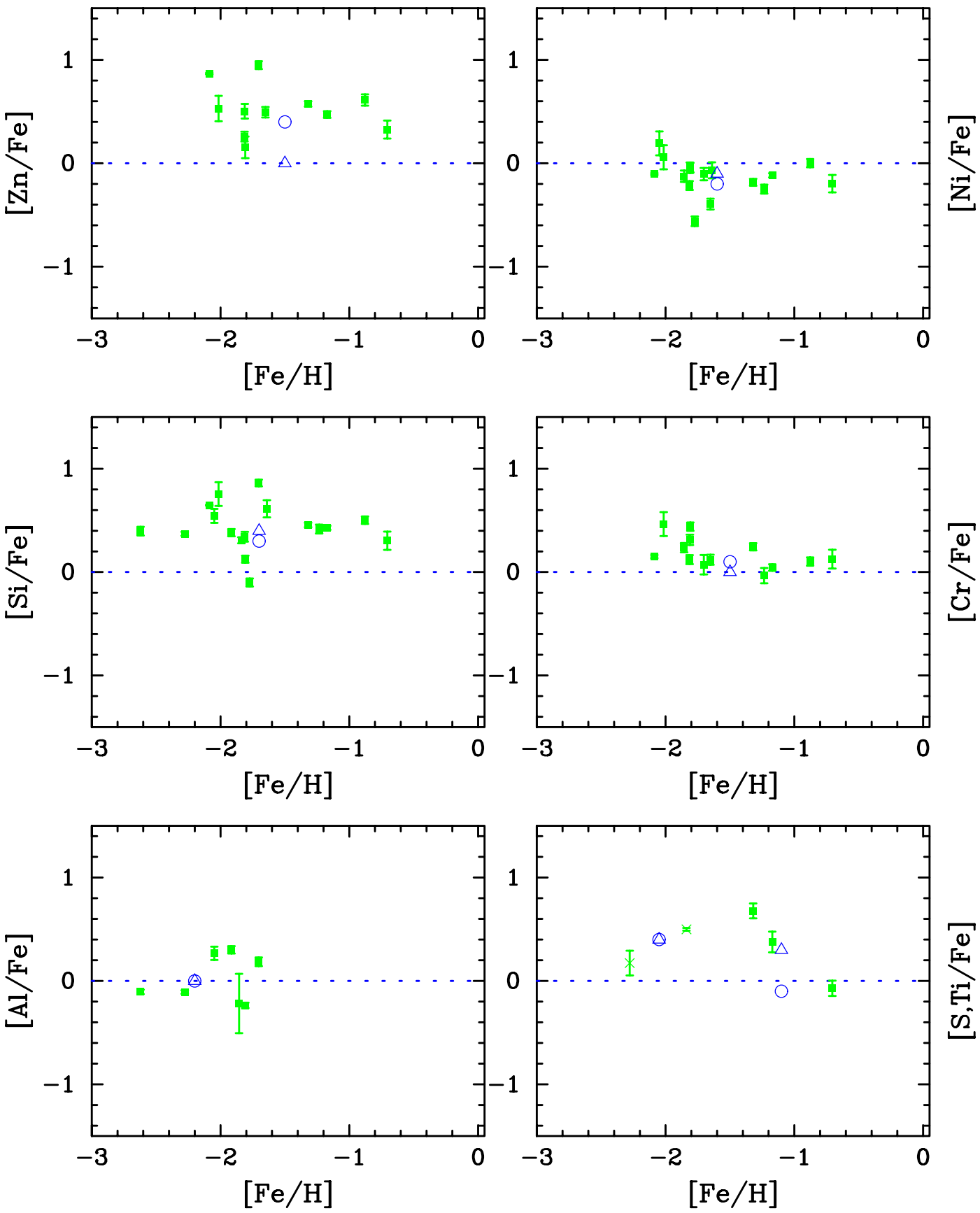

FIG. 22.—Abundance patterns of the most common elements from our full damped Lyα sample. Following standard practice in stellar abundance analysis we plot [X/Fe], the logarithmic abundance of element X to Fe relative to solar. We plot this quantity vs. [Fe/H], an indicator of the metallicity of the system. The triangles printed in each panel represent the typical metal-poor halo value (McWilliam 1997). The circles indicate the observed pattern for lightly depleted ISM gas (Savage & Sembach 1996). In the lower right panel, the crosses identify [S/Fe] values and the squares mark [Ti/Fe].

sized by Lu et al. (1996), the overabundance[3] of Si/Fe relative to solar is very suggestive of Type II supernova enrichment (McWilliam 1997). In the case of Si/Fe, the Si overabundance is explained as the result of the overproduction of Si—an α element relative to Fe in Type II supernovae. Similarly, the Cr/Fe and Al/Fe patterns are consistent with those observed for the metal-poor halo stars. Contrary to the Lu et al. observations, however, we observe an overabundance of Cr/Fe at very low metallicity (for [Fe/H] < -1.5, $\langle$[Cr/Fe]$\rangle = +0.21$). This result is most likely due to the fact that we are biased to high [Cr/Fe] values at low [Fe/H] because low [Cr/Fe] values would imply Cr^+ column densities below our detection limit. In one system (Q0149+33) we observe [Cr/Zn] > 0 dex, which indicates that it is essentially undepleted by dust grains. Furthermore, we measure an overabundance of Si relative to Fe in this system ([Si/Fe] $= +0.12$ dex), which is an indication of a Type II α, enhancement although at a somewhat smaller level than most metal-poor halo stars. Finally, although the [Al/Fe] measurements are broadly consistent with the abundances observed in metal-poor halo stars, there may be a contradiction at very low [Fe/H]. For halo stars with [Fe/H] < -2 dex, [Al/Fe] < -0.4 dex (McWilliam 1997) yet if anything the damped Lyα systems exhibit [Al/Fe] > 0 dex at this metallicity. This result may ultimately pose a serious challenge to the interpretation of Type II SN nucleosynthetic patterns.

Although the abundances for Cr, Al, and Si versus Fe resemble those for the metal-poor halo stars, the patterns also tend to match the dust-depletion patterns of lightly depleted regions within the ISM (Savage & Sembach 1996). In these regions, Si is overabundant relative to Fe, [Cr/Fe] ≈ 0.1 dex, and recent measurements of the Al to Fe ratio toward three OB stars (Howk & Savage 1999) suggest [Al/Fe] $\gtrsim 0$ dex. If the overabundance of Si/Fe relative to solar is indicative of dust depletion, then one might expect a correlation between [Si/Fe] and [Zn/Fe] with the most heavily depleted regions showing the largest Si/Fe and Zn/Fe ratios. A plot of [Si/Fe] versus [Zn/Fe] for all the systems with accurate abundances for the three elements (Fig. 23) reveals a positive correlation (the Pearson coefficient is 0.86 in log space with a null hypothesis probability of 0.003), consistent with that expected for dust depletion. However, if Zn is produced in the neutrino-driven winds of Type II SNe (Hoffman et al. 1996), one may also expect a correlation between the abundance of Si and Zn relative to Fe.

Now consider the observations of Ti/Fe (*solid squares in the lower right hand panel*), which pose a strong argument for Type II SN enrichment. As emphasized in Prochaska & Wolfe (1997a), Ti is more heavily depleted than Fe in dusty regions within the ISM (Lipman & Pettini 1995), yet we find [Ti/Fe] ≥ 0 in every damped Lyα system where Ti is observed. As Ti is an α element, this argues strongly for the Type II SN interpretation. Lu et al. (1996) have made similar arguments for the observed underabundance of Mn/Fe in the damped systems. Because Mn is less depleted than Fe in dusty regions of the ISM, the Mn/Fe underabundance cannot be explained by dust depletion. On the other hand one observes [Mn/Fe] < 0 dex for the metal-poor halo stars (McWilliam 1997). Furthermore, the

[3] The one data point with [Si/Fe] < 0 is from Q0000−26 where both the Si^+ and Fe^+ column densities are insecure.

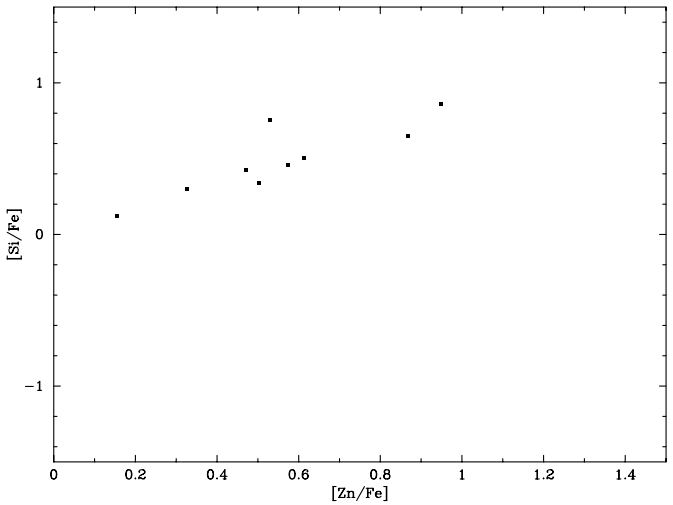

FIG. 23.—[Si/Fe], [Zn/Fe] pairs for the nine damped Lyα systems from the full sample exhibiting Si, Zn, and Fe. The positive correlation (Pearson's correlation coefficient $r = 0.86$ with the null hypothesis a 0.003 probability) is suggestive of dust depletion but could possibly have a nucleosynthetic origin (see text).

[Mn/Fe] values show a similar trend with [Fe/H] (albeit in terms of an underabundance) to that of the α elements. It is possible that this trend indicates a metallicity dependent yield for Mn, but the plateau in [Mn/Fe] values at [Fe/H] ≈ -1 to -2.5 is better understood if Mn is overproduced relative to Fe by Type Ia supernovae (Nakamura et al. 1999). If the latter explanation is correct, then the low [Mn/Fe] values are significant evidence for Type II SN enrichment within the damped Lyα systems. At the very least, we wish to stress that the damped [Mn/Fe] observations require that the underlying nucleosynthetic pattern does not simply match solar abundances.

For the elements considered thus far, the abundance patterns are broadly consistent with a combination of Type II SN enrichment and an "ISM-like" dust-depletion pattern. This is not the case for sulphur. In the two cases from our full sample where we have accurate measurements for S/Fe we find (1) [S/Fe] $= 0.50 \pm 0.02$ for the damped system at $z = 3.025$ toward Q0347−38 and (2) [S/Fe] $= 0.17 \pm 0.1$ for the damped system toward Q2348−14. Similar to silicon, sulfur is an α element and is observed to be overabundant relative to Fe in metal-poor halo stars by $[Si/Fe]_{II} \approx 0.3$–0.5 dex. Like zinc, sulfur is undepleted in the ISM. Therefore, interpreting the positive [Zn/Fe] values as the result of dust depletion, one would expect typical values for $[S/Fe]_{dust} > 0.3$ dex on the basis of depletion alone. Given that all of the damped systems—including those from Lu et al. (1996)—exhibit [S/Fe] ≤ 0.5 dex, the S abundance pattern is inconsistent with a combination of Type II SN enrichment and dust depletion because this would require $[S/Fe]_{obs} = [S/Fe]_{II} + [S/Fe]_{dust} > 0.6$ dex in every case. Although this point has been discussed previously, it needs to be emphasized. If dust is playing the primary role in the observed abundance patterns of the damped Lyα systems, then the [S/Fe] measurements require one of two conclusions: (1) the damped Lyα systems were *not* primarily enriched by Type II SNe, or (2) all of the systems where S has been measured are atypical in that they are the few that are undepleted. The first conclusion is at odds with most theories of galactic chemical evolution and is inconsistent

with the observations of the Milky Way. To adopt point (1), one would have to argue that the chemical history of the damped systems is very different from that of the Milky Way. Point (2) is a possibility for Q2348−14, but the Ni/Fe ratio observed for Q0347−38 ([Ni/Fe] < −0.5) would indicate that this system is significantly depleted. At present, then, any attempt to match the abundance patterns of the damped Lyα systems with a combination of Type II SN enrichment and ISM-like dust depletion must fail the S observations.

Synthesizing our results with those from previous studies, we contend the abundance patterns of the damped Lyα systems lack any convincing single interpretation. On the face of it this may not be surprising, as one would expect some differences in their chemical evolution. Although this would explain variations of a particular X/Fe ratio, it is unlikely to account for any of the inconsistencies discussed thus far. Although the majority of the patterns are in excellent agreement with the Type II SN enriched halo star abundance patterns, Zn/Fe and Ni/Fe are clearly inconsistent and are very suggestive of dust depletion, albeit at considerably lower levels than that observed in dusty ISM clouds. An ISM-like dust-depletion pattern on top of solar abundances accounts for a majority of the observations but fails for Mn/Fe and Ti/Fe. Attempts to match the observed abundance patterns with a combination of dust depletion and Type II supernova enrichment have been largely unsuccessful (Lu et al. 1996; Kulkarni et al. 1997; Vladilo 1998). This failure is accentuated by our measurements of [S/Fe], which are inconsistent with a synthesis of dust depletion and Type II SN abundance patterns. Of course to eliminate either effect would have profound consequences. If the damped Lyα systems do not exhibit Type II SN abundances, they have a very different chemical evolution history than the Milky Way in that they do not match the stellar abundance patterns for [Fe/H] < −1 dex. This would raise the questions: Is the Milky Way unique? Or do the damped Lyα systems somehow not include the progenitors of present-day spiral galaxies? Also, why would the damped systems exhibit relative solar abundances for all elements except Mn and Ti? On the other hand, if there is no dust depletion at play, then is the Zn/Fe ratio observed in the Milky Way a special case? Also, are the [Al/Fe] observation at low metallicity consistent with the Type II SN interpretation?

At the heart of these questions lies the physical nature of the damped Lyα systems. If dust depletion is playing a principal role, then perhaps the damped systems are tracing gas-rich galaxies not unlike the Magellanic Clouds (Welty et al. 1997), whereas an underlying Type II SN pattern is more suggestive of the progenitors of massive spiral galaxies. What steps can be taken to resolve these issues? First, the overabundance of Ti/Fe must be confirmed. A more accurate measurement of the Ti II λ1910 f values would be particularly useful. This could be achieved by performing observations of a system showing both the Ti II λ1910 and Ti II λ3073 transitions. Unfortunately, at present this requires high-S/N, high-resolution observations at wavelengths exceeding 9000 Å (i.e., $z \approx 2$). One could much more easily measure [Ti/Fe] in a few low-z systems via the Ti II λ3073 transition, but the majority of these systems exhibit [Fe/H] > −1 dex (Pettini et al. 1999) and therefore may not offer a fair comparison with the metal-poor halo stars. It is interesting to note, however, that the presumed damped system at $z = 0.75$ toward Q2206−19 has [Ti/Fe] = 0.27 dex, which indicates an underlying Type II SN abundance pattern (Prochaska & Wolfe 1997a). Second, one can look to the relative abundances of the α elements S, Si, O, and Ti to investigate consistency with the metal-poor halo star patterns. Thus far the few data points we have are consistent with the Type II SN interpretation ([S/Si] ≈ 0.2 dex and [Si/Ti] ≈ 0.1 dex). Third, the conclusions we have drawn from the S/Fe ratio are based on very few damped Lyα systems. Given the importance of this particular ratio, further measurements of sulphur would be particularly enlightening. Finally, a more detailed abundance analysis of the lowest metallicity systems would allow one to investigate the chemical evolution of the damped systems. Assuming that the extremely metal-poor systems are the least depleted, they should provide the most accurate indication of the underlying nucleosynthetic pattern.

5. METALLICITY

We now turn to examine the metallicity of our sample of damped systems. Given the debate on the presence of dust in the damped Lyα systems, we will consider both Zn/H and Fe/H. Figure 24 plots our complete sample of [Zn/H] and [Fe/H] measurements versus redshift. The column density-weighted mean for Zn,

$$\left[\left\langle\frac{\mathrm{Zn}}{\mathrm{H}}\right\rangle\right] = \log\frac{\sum_i N(\mathrm{Zn}^+)_i}{\sum_i N(\mathrm{H}^0)_i} - \log\left(\frac{\mathrm{Zn}}{\mathrm{H}}\right)_\odot , \qquad (2)$$

for our full sample is $[\langle \mathrm{Zn/H} \rangle] = -1.15 \pm 0.15$ dex.[4] This result confirms that of Pettini et al. (1997). For Fe, we find $[\langle \mathrm{Fe/H} \rangle] = -1.64 \pm 0.11$ dex for $z < 3$ and -1.77 ± 0.11 dex for $z > 3$. Lu, Sargent, & Barlow (1997) have used similar measurements (in fact several of the values presented here) to conclude that $z \approx 3$ marks the onset of significant star formation in the damped Lyα systems. Their interpretation is based on the fact that the damped systems exhibit a

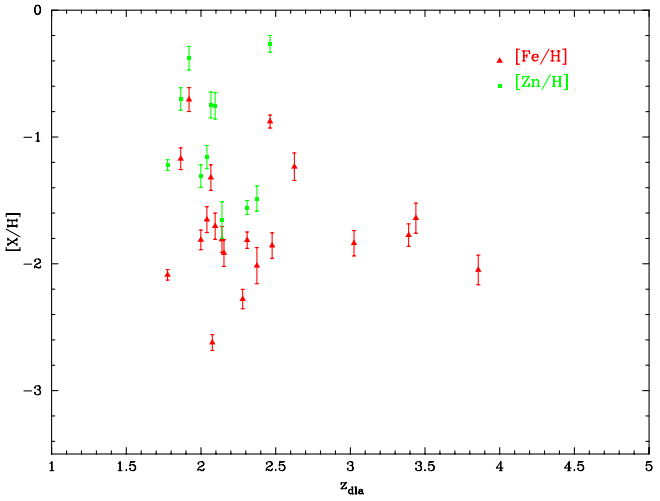

FIG. 24.—[Zn/H] and [Fe/H] measurements from the full sample of damped Lyα systems vs. redshift. The increase in [Fe/H] for $z < 3$ may indicate the onset of star formation in the damped Lyα systems.

[4] Note that the error estimate reflects the errors in the individual [Zn/H] measurements and not the size of the data sample.

break in [⟨Fe/H⟩] at $z \approx 3$. Formally, our data do not support their conclusion, but the fact that the high-redshift [⟨Fe/H⟩] value is dominated by only three systems (Q0000−26, Q0019−15, and Q0347−38) suggests that our result is probably suffering from small number statistics.

6. SUMMARY AND CONCLUSIONS

We have presented accurate ionic column density and abundance measurements for 19 damped Lyα systems observed with HIRES on the 10 m W.M. Keck Telescope. Throughout the paper we have used the apparent column density techniques to analyze the damped Lyα profiles and have adopted N(H I) values from the literature. The main results of the paper are summarized as follows.

1. The abundance patterns of our 19 systems match those observed by Lu et al. (1996). Therefore, our analysis confirms their primary conclusion that the damped Lyα systems exhibit abundance patterns representative of Type II SN enrichment with the major exception of [Zn/Fe] and to a lesser extent [Ni/Fe]. The Zn and Ni patterns, however, are in accordance with what one would expect for dust depletion based on observations of the lightly depleted, "warm" H I clouds in the ISM. Although the combination of dust depletion and Type II SN enrichment fits the majority of the observations, this interpretation is ruled out by the observed values of [S/Fe].

2. A majority of the damped Lyα elemental abundances are consistent with a dust-depletion pattern on top of an underlying solar abundance pattern. Observations of titanium and manganese, however, strongly contradict this interpretation. In every system where Ti is observed, we measure [Ti/Fe] ≥ 0 dex consistent with the observed overabundance found in metal-poor halo stars and therefore suggestive of Type II SN enrichment. Similarly, the observed underabundance of [Mn/Fe] (Lu et al. 1996) is opposite to the effects of dust depletion and therefore requires a nucleosynthetic explanation, albeit not necessarily Type II SN yields.

3. Our metallicity measurements confirm the principal results from the surveys of Pettini and collaborators. Specifically, we find [⟨Zn/H⟩] $= -1.15 \pm 0.15$ dex, [⟨Fe/H⟩] $= -1.64 \pm 0.11$ dex for $z < 3$, and -1.77 ± 0.11 dex for $z > 3$. Although we do not observe an evolution in the column density-weighted Fe abundance with redshift—as claimed by Lu et al. (1997)—we expect that this inconsistency lies in the small number statistics of our high-z sample.

4. For a number of damped Lyα systems in our sample (e.g., Q1331, Q0201, Q2348), we observe metal-line systems within 500 km s^{-1} of the damped system. In the case of Q2348, for example, a metal-line system exhibiting Si II, Si IV, and Al III transitions is located only 100 km s^{-1} from the strongest damped Lyα component. The absence of Fe II and O I absorption and the Si II/Si IV ratio for this component, however, indicates that this system is significantly ionized. We believe that the same is true for the majority of these neighboring metal-line systems (the system at $z = 1.858$ toward Q2230+02 is a notable exception). If they were identified independently of the damped system, these systems would be very strong Lyman limit systems. Their coincidence with the damped system suggests that they lie within the halo enclosing the damped system or perhaps that of a neighboring protogalactic system. We expect that a detailed analysis of these systems may provide important insight into the physical conditions surrounding the damped Lyα systems.

We thank the group headed by W. L. W. Sargent including Limin Lu for generously providing us with their HIRES spectra. We acknowledge very helpful discussions with A. McWilliam, M. Pettini, and G. Fuller. We also would like to thank L. Storrie-Lombardi and I. Hook for helping to provide target lists and N(H I) measurements. We acknowledge the very helpful Keck support staff for their efforts in performing these observations. A. M. W. and J. X. P. were partially supported by NASA grant NAGW-2119 and NSF grant AST 86-9420443.

REFERENCES

Briggs, F. H., Wolfe, A. M., Liszt, H. S., Davis, M. M., & Turner, K. L. 1989, ApJ, 341, 650
Evardsson, B., Anderson, J., Gutasfsson, B., Lambert, D. L., Nissen, P. E., & Tompkin, J. 1993, A&A, 275, 101
Fall, S. M., & Pei, Y. C. 1993, ApJ, 402, 479
Ferland, G. J. 1991, Ohio State Univ. Internal Report 91-01
Hoffman, R. D., et al. 1996, ApJ, 460, 478
Howk, J. C., & Savage, B. D. 1999, ApJ, submitted
Kulkarni, V. P., Fall, S. M., & Truran, J. W. 1997, ApJ, 484, 7
Lipman, K., & Pettini, M. 1995, ApJ, 442, 628
Lu, L., Sargent, W. L. W., & Barlow, T. A. 1997, ApJ, 484, 131
Lu, L., Sargent, W. L. W., Barlow, T. A., Churchill, C. W., & Vogt, S. 1996, ApJS, 107, 475
Malaney, R. A., & Chaboyer, B. 1996, ApJ, 462, 57
McWilliam, A. 1997, ARA&A, 35, 503
Morton, D. C. 1991, ApJS, 77, 119
Nakamura, T., Umeda, H., Nomoto, K., Thielemann, F., & Burrows, A. 1999, ApJ, in press (astro-ph/9809307)
Pettini, M., Ellison, S., Steidel, C. C., & Bowen, D. V. 1999, ApJ, 510, 576
Pettini, M., Lipman, K., & Hunstead, R. W. 1995, ApJ, 451, 100
Pettini, M., Smith, L. J., Hunstead, R. W., & King, D. L. 1994, ApJ, 426, 79
Pettini, M., Smith, L. J., King, D. L., & Hunstead, R. W. 1997, ApJ, 486, 665
Prochaska, J. X., & Wolfe, A. M. 1996, ApJ, 470, 403
———. 1997a, ApJ, 474, 140
Prochaska, J. X., & Wolfe, A. M. 1997b, ApJ, 486, 73
———. 1998, ApJ, 507, 113
Savage, B. D., & Sembach, K. R. 1991, ApJ, 379, 245
———. 1996, ARA&A, 34, 279
Sneden, C., Gratton, R. G., & Crocker, D. A. 1991, A&A, 246, 354
Songaila, A., et al. 1994, Nature, 371, 43
Storrie-Lombardi, L. J., & Wolfe, A. M. 1999, in preparation
Storrie-Lombardi, L. J., McMahon, R. G., & Irwin, M. J. 1996, MNRAS, 283, L79
Tripp, T. M., Lu, L., & Savage, B. D. 1996, ApJS, 102, 239
Viegas, S. M. 1994, MNRAS, 276, 268
Vladilo, G. 1998, ApJ, 493, 583
Vogt, S. S. 1992, in ESO Conf. and Workshop Proc. 40, High Resolution Spectroscopy with the VLT, ed. M.-H. Ulrich (Garching: ESO), 223
Welty, D. E., Lauroesch, J. T., Blades, J. C., Hobbs, L. M., & York, D. G. 1997, ApJ, 489, 672
Wolfe, A. M., & Davis, M. M. 1979, AJ, 84, 699
Wolfe, A. M., Fan, X.-M., Tytler, D., Vogt, S. S., Keane, M. J., & Lanzetta, K. M. 1994, ApJ, 435, L101
Wolfe, A. M., Lanzetta, K. M., Foltz, C. B., & Chaffee, F. H. 1995, ApJ, 454, 698
Wolfe, A. M., & Prochaska, J. X. 1998, ApJ, 494, L15
Wolfe, A. M., Turnshek, D. A., Smith, H. E., & Cohen, R. D. 1986, ApJS, 61, 249
Zsargó, J., & Federman, S. R. 1998, ApJ, 498, 256